GRAVITY WAVES IN TITAN'S ATMOSPHERE

A. James Friedson

MS 169-237, Jet Propulsion Laboratory
California Institute of Technology
Pasadena, CA 91109
email: ajf@maui.jpl.nasa.gov

Submitted to *Icarus*, July 9, 1993
Revised, December 10, 1993

Manuscript Length: 29 pages, 9 figures, O tables.

PROPOSED RUNNING HEAD:

GRAVITY WAVES IN TITAN'S ATMOSPHERE

Send editorial correspondence and proofs to:

A. James Friedson
Mail Stop 169-237
Jet Propulsion Laboratory
4800 Oak Grove Drive
Pasadena, CA 91109

Telephone: (818)-354-2397
Fax: (818)-393-4619

Abstract

Scintillations (high frequency variations)) observed in the radio signal during the occult ation of Voyager 1 by Titan (Hinson and Tyler 1983) provide information concerning neutral atmospheric density fluctuations on scales of hundreds of meters to a few kilometers. Those seen at altitudes higher than 25 km above the surface were interpreted by Hinson and Tyler as being caused by linear, freely propagating (energy-conserving) gravity waves, but this interpretation was found to be inconsistent with the scintillation data below the 25 km altitude level. Here an attempt" is made to interpret the entire scintillation profile between the surface and the 90 km altitude level in terms of gravity waves generated at the surface, Numerical calculations of the density fluctuations caused by two-dimensional, nonhydrostatic, finite-amplitude gravity waves propagating vertically through Titan's atmosphere are performed to produce synthetic scintillation profiles for comparison with the observations. The numerical model accurately treats the effects of wave transience, nonlinearity, and breakdown due to convective instability in the overturned part of the wave, The results indicate that wave phase speeds could not have exceeded 2 m see-l and must have been oriented in the meridional (north-south) direction if there are strong zonal winds on Titan. The high altitude scintillation data were accurately recovered with a freely propagating wave solution, confirming the analytic model of Hinson and Tyler (1983). The amplitude, phase speed, and horizontal and vertical wavelengths of the freely propagating waves are consistent with their having been generated in the convective boundary layer at Titan's surface. It is found that the low altitude scintillation data can be fit by a model where a component of the gravity waves becomes connectively unstable and breaks near the 15 km level. A definitive value for the amplitude of the breaking wave can not be obtained without better knowledge of its horizontal wavelength and phase speed. If the breaking wave had the same horizontal wavelength, approximately 4 km, as the freely propagating waves, then its vertical perturbation velocity near the surface would have been ~ 1.4 cm see-l , and its phase speed would have been ~ 20 cm see^{-1} . This component could also have been generated by convection near the surface, Alternatively, it is estimated that the breaking wave could have been forced by topographic relief of 60-300 meters. The large-scale structure of the observed scintillation profile in the entire altitude range between 5 and 85 km can bc simulated by a model where the freely propagating and breaking waves are forced at the surface simultaneously, Further analysis of the Voyager 1 Titan low-altitude scintillation data, using inversion theory appropriate for strong scattering, could potentially remove some of the ambiguities remaining in this analysis and allow for a better determination of the strength and source of the waves.

Introduction

A recent analysis of the central flash contained in stellar occultation data has provided strong evidence that Tit an possesses a global system of cyclostrophically balanced, superrotating winds near the 0.25 mbar pressure level, with zonal winds of ~ 170 m see–l at high latitudes dropping to near 100 m sec^{-1} at the equator (Hubbard et al. 1993). These results are in accord with a previous estimate based on the equator-to-pole temperature difference in the stratosphere and the assumption of cyclostrophic balance (Hunten et al. 1984). To understand the balance of forces required to maintain this system of winds necessitates learning more about the torques created by waves and eddies in Titan's atmosphere.

Unfortunately, the data base concerning properties of waves and eddies in Titan's atmosphere is not extensive. The haze in Titan's atmosphere prevented the location of distinct cloud features for the purposes of measuring winds, and the Voyager 1 IRIS experiment failed to detect the thermal signature of any eddies down to horizontal scales $\sim 30°$ in longitude; an upper limit of 1 K was assigned to longitudinal temperature variations at the tropopause, and 3 K in the upper stratosphere (Flasar et al. 1981). On the brighter side, the Voyager 1 radio occultation experiment has provided useful information concerning atmospheric density fluctuations occurring on spatial scales between a few hundred meters to a few kilometers. These fluctuations are thought to be evidence of vertically propagating gravity waves (Hinson and Tyler 1983; hereafter HT), and as such potentially serve as a probe of the background atmospheric structure (wind and stratification) and of the mechanisms which excite the waves, The purpose of this paper is to build upon Hinson and Tyler's gravity wave interpretation of the radio occultation data, extending it to the troposphere and placing it on a more quantitative footing.

As the Voyager 1 spacecraft was occulted by Titan in November 1980, the path of the radio beam through the satellite's atmosphere was affected by spatial inhomogeneity in the gas refractivity. The large scale variation of the refractivity was analyzed to produce vertical profiles of molecular number density, pressure, temperature, and microwave absorption (Tyler et al 1981; Lindal et al 1983). Small-scale refractivity variations led to high-frequency fluctuations, or scintillations, in the radio signals received at Earth. Since refract ivit y is proportional to density for non-polar gases, the scintillations contain information about density irregularities in Titan's atmosphere ranging from a few hundred meters to a few kilometers in scale.

HT computed a power spectrum for the scintillations observed at the 44 km altitude level and determined that the density fluctuations to which the experiment was sensitive were characterized by a horizontal to vertical scale ratio of 4:1, a dominant vertical scale of ~ 1 km, and a RMS fractional variation in the density of 10^{-3}. They also determined a vertical profile for the scintillation index, a quantity proportional to the variance of refractivity irregularities and hence also proportional to the variance of fluctuations in atmospheric density. Between 25 and 90 km, the scintillation index was found to vary with altitude approximately as $\rho_0 N^4$, where ρ_0 is the basic state density and N is the Brunt frequency associated with the basic state stratification. HT argued that this profile

is exactly that expected of the density fluctuations caused by vertically propagating gravity waves of constant energy flux, the amplitude of which increases with altitude in proportion to $\rho_0^{-1/2}$. Below 25 km, in the troposphere, the scintillation index was found to decrease with altitude faster than expected for freely propagating waves; in fact, the profile in this region was roughly consistent with one in which waves maintained a constant amplitude as they propagated upward. In addition, the scintillations were much stronger and more variable with altitude than in the region above 25 km. These differences led HT to discard the gravity wave model for the troposphere, and they instead proposed that refractivity variations arising from layered clouds or stratified layers in clear air might be the source of the strong scintillations below 25 km. They did not attempt to demonstrate that either of these effects would reproduce the observed scintillation profile.

Ross et al. (1989) suggested that HT may have been too quick to discard the gravity wave explanation for the troposphere. They noted that the region of low static stability below 25 km would serve as a low pass filter to gravity waves. Gravity waves are able to propagate vertically only if their doppler-shifted frequency (that is, the wave frequency as measured in the local rest frame of the gas) is less than the local Brunt frequency N associated with the static stability. otherwise they are evanescent (their amplitude decays exponentially with altitude). It was suggested that the altitude dependence of the scintillations observed between 5 and 25 km could be explained if they were caused by vertically attenuated waves, generated near the surface, with periods lying between about 0.5 and 2.5 hours. Waves with periods much shorter than 0.5 hour would be too strongly attenuated, while waves with periods much longer than 2.5 hours would grow too quickly with altitude to fit the data. Ross et al. also argued that if there is indeed a system of cyclostrophic zonal winds in Titan's atmosphere, as implied by the meridional temperature gradients and stellar occultation data, then the phase speed of the waves causing the scintillations would have to be oriented in the meridional (north-south) direction, Otherwise, the waves would be absorbed at critical layers (where the doppler-shifted phase speed goes to zero) or would be doppler-shifted to a frequency well above the cutoff frequency associated with the static stability at some altitude in the troposphere or stratosphere.' This is a significant point, since the waves in HT's model for stint illations at the 44 km altitude level (upper troposphere) have phase speeds of only $\sim$1 m see^{-1}, much smaller than the $\sim$25 m sec^{-1} zonal wind estimated for the troposphere and $\sim$75 m see^{-1} zonal wind estimated for the upper stratosphere from cyclostrophic balance (Hunten et al. 1984), Meridionally traveling waves, on the other hand, would be unaffected by the zonal wind, and by the same token, would play no role in forcing the zonal wind.

It will be shown in Section 3 that evanescent waves could not in fact have been responsible for the scintillations in the troposphere. Mechanisms other than evanescence, such as wave transience, wave breaking, or propagation through a background meridional wind that varies with altitude, may also lead to slow wave amplitude growth or amplitude decay wit h height, and may offer a consistent explanation of the data. Here we conduct numerical calculations of nonlinear, two-dimensional, nonhydrost at ic gravit y wave propagat ion through Titan's atmosphere in an attempt to simulate the scintillation index vertical profile and to assess the effects of evanescence, wave transience, and wave breaking on the

profile in the troposphere. The primary goal is to formulate a model to account for the vertical variation of scintillation index, between the surface and 90 km, entirely in terms of gravity waves generated near the surface. A successful simulation has the potential to yield valuable information concerning the source of the waves and their role in the atmospheric circulation, The principal challenge is to simultaneously produce near-constant wave amplitudes in the lower troposphere and free, energy flux-conserving propagation at higher altitudes. It is shown below that the most success in fitting the scintillation observations is obtained with a model in which both a freely propagating wave and a wave that breaks at an altitude of 15 km are generated simultaneously near the surface.

The next section describes the formulation of the model, discussing the equations of motion that are solved, the numerical method used, the background atmosphere, the forcing of the waves at the lower boundary, the dissipative "sponge layer" at the upper boundary, and the convective adjustment scheme which becomes operative when the waves grow to such an amplitude that they become connectively unstable and break. The results arc presented in Section 3, and their implications for the nature of gravity waves in Tit an's atmosphere and their generation are discussed in Section 4.

2. Model Formulation

a. *Basic State*

The background atmospheric thermal structure will generally assert a significant influence over gravity wave propagation, since the amplitude and vertical wavelength of a vertically propagating packet will continually adjust in response to vertical variations of the static stability. Fortunately, the vertical profiles of mean temperature, density, and pressure at low latitudes have been characterized quite well by the Voyager 1 radio occultation experiment (Lindal et al, 1983). 'l'he data are most reliable between the surface and $\sim$100 km; above, the measurements become increasingly sensitive to the initial conditions assumed in the data analysis. There is some small uncertainty regarding the absolute scale of the temperature measurements, related to the fact that the experiment actually measured the ratio of temperature to mean molecular weight rather than temperature directly. This uncertainty has only a very minor impact on the static stability profile and hence very little effect on the propagation of the gravity waves.

The background vertical profiles of temperature and Brunt frequency used in the calculations are shown in Figure 1. The temperature profile between O and 150 km was taken from the table created by Lindal et, al. (1983). Above 150 km, the adopted profile is warmer than Lindal et al.'s nominal result and corresponds to the warmest temperatures allowed within existing observational constraints (see Appendix B of "Cassini Mission: Saturn Orbiter Proposal Information Package", Vol. 2, 1989). Results presented in Section 3 were found to be insensitive to details of the thermal structure above 150 km; this was verified by running cases in which Lindal et al.'s nominal profile was used for temperatures above 150 km and comparing the results to those obtained using the profile shown in Fig. 1. The Brunt frequency was calculated from the temperature profile according to

$N(z) = [(g/T)(\partial T/\partial z + g/C_p)]^{1/2}$, where T is temperature, z altitude, g = 135 cm sec^{-2} is Tit an's gravit at ional acceleration, and C_p is t he specific heat at constant pressure of a pure nitrogen atmosphere. The low values of N at low altitudes reflect the nearly adiabatic lapse rates there, while the peak of N near 68 km occurs as a consequence of the strong thermal inversion at this altitude.

The radio occultation data indicate lapse rates very close to adiabatic occurring below the 3-4 km level. These are probably associated with a well-mixed layer of buoyancy-driven turbulence (Hunten et al, 1984). In the model, the very low values of N implied by the near-adiabatic lapse rates below 4 km have been replaced by the somewhat larger values shown in Fig. 1. The purpose of this replacement is to simplify the calculation of forcing at the lower boundary, in particular preventing the production of breaking waves in the mixed layer, which is not of physical interest here and which leads rapidly to numerical instability in the computations, In the actual atmosphere, gravity waves owing their existence to convection near the surface will be generated at the interface at 4 km between the mixed layer and the stably stratified layer lying immediately above the mixed layer. In the model, the forcing of such waves can be adequately simulated by generating the waves at the surface in the presence of the basic state stratification shown in Fig. 1. Since the amplitude of a freely propagating wave at 4 km will differ from the amplitude at O km by only 10%, forcing the wave at the surface in the numerical model is essentially equivalent to forcing it at 4 km, apart from an unimportant phase difference. Hence, the wave solutions presented below are equivalent to those that would be obtained had the lower boundary condition been imposed at the 4 km altitude level instead of the surface. Naturally, the wave solutions obtained by the model for altitudes below 4 km will be affected by the artificial stratification that has been introduced there, and hence no attempt is made to compare model results to the radio occultation observations below 4 km. In particular, none of the conclusions drawn from the calculations in this paper depend upon the choice for the stratification in the lowest 4 km. The effect that the observed stratification would have on topographically forced waves is discussed in Section 4.

The stellar occultation measurement of strong equatorial zonal winds of $\sim$100 m sec^{-1} at 0.25 mbar pressure (Hubbard et al. 1993), the inference of zonal winds of $\sim$75 m see^{-1} in the upper stratosphere from Voyager 1 IRIS thermal measurements, and our experience with Venus' circulation and the fact that Venus and Titan are expected to have similar meteorologies (Hunten et al. 1984) all suggest that Titan possesses a global system of appreciable zonal winds. However, there are no direct measurements of zonal winds in Titan's troposphere. An inferred equator-to-pole temperature difference of $\sim$2 K in the lower troposphere and the assumption of cyclostrophic balance led Hunten et al. (1984) to estimate zonal winds there to be about 25 m see–l . Later, Toon et al. (1988) challenged this estimate, arguing that the meridional temperature contrast, and hence the magnitude of the zonal wind, may have been overestimated, It is likely that the true magnitude of the tropospheric zonal winds will not be known until measurements from the Cassini mission to Saturn are in hand. To make progress in interpreting the scintillations in terms of gravity waves, some assumption must be made regarding the nature of the winds at the equator, Here the view has been taken that vertical shears, large enough to lead to wind

differences at different altitudes of a few meters per second or more, probably exist in the lower atmosphere, implying that the scintillations were most likely caused bymeridionally propagating waves. It must be emphasized, however, that thcrcsults presentedin Section 3 are strictly applicable only when the wave propagation is unaffected by the background zonal wind, This would be the case if the waves propagated in the meridional direction or if zonal winds in the lower atmosphere were much less than ~ 1 m sec^{-1}. If, on the other hand, a weak vertical wind shear exists in the troposphere, then the possibility arises that zonally propagating waves may have interacted with a critical layer somewhere between the ~ 10 and 30 km altitude levels, This type of interaction is not included in the present calculations; however, for such a situation to have occurred requires a very weak vertical shear, such that zonal winds do not change by more than ~ 2 m see-l over an altitude range of tens of kilometers.

Meridionally propagating waves would be unaffected by zonal winds but would be affected by a background meridional wind. Flasar et al, (1981) estimated zonal mean meridional velocities in the lower troposp.here and upper stratosphere by considering the equator-to-pole thermal energy balance. The characteristic meridional velocities they obtained were ~ 0.04 cm sec^{-1} for the lower t roposphcre and ~ 2 cm sec^{-1} for the upper stratosphere. These values are much lower than the phase speed (~ 1 m see-l) of the gravity waves inferred by HT, and so it appears very unlikely that the zonal mean meridional velocity played a significant role in the gravity wave propagation. It can not be stated with certainty that *local* values of the meridional velocity could not have been substantially larger than the zonal means and so have affected local wave propagation, especially in the upper stratosphere, but we have no way to quantify this at present. For the purposes of the present calculations, it is assumed that the background meridional wind had a negligible effect on meridional wave propagation.

b. Wave Parameters

It is assumed in the model that the waves are forced at or very near Titan's surface. As mentioned in the previous section, the region of low static stability in the troposphere causes waves with periods shorter than about 0.5 hour to suffer severe vertical attenuation, hence the primary focus will be on waves with periods greater than 0.5 hour. HT found the dominant horizontal length scale of the density fluctuations at the 44 km altitude level to be ~ 4 km and the dominant vertical scale to be ~ 1 km. These were interpreted as the dominant horizontal and vertical wavelengths of the gravity wave spectrum. Together with the value of the Brunt frequency at 44 km, $N = 5 \times 10^{-3}$ see-l, they imply a phase speed of ~ 1 m see–l . HT did not determine the spatial scale of the density variations below the 25 km level. For gravity waves which are not strongly nonlinear, propagating through an atmosphere where the fractional variation of the Brunt frequency on horizontal surfaces is small, the phase speed measured relative to the surface and the horizontal wavelength of a vertically propagating wave packet arc nearly conserved, changing only to the extent that the projection of the ambient wind vector along the wavevector changes in the direction parallel to the wavevector (Lighthill 1978). Therefore, fo, meridionally propagating waves, the horizontal wavelength and phase speed will remain nearly constant if the background

meridional wind that the wave packet passes through over its lifetime changes very little, We find that this condition is satisfied in general in the model for zonal mean meridional winds less than a few centimeters per second and for a spatial scale of the background meridional wind on the order of a Titan radius (Hunten et al. 1984), On this basis, we assume the horizontal wavelength to be nearly conserved during propagation and require that the waves forced near the surface have a horizontal wavelength of $\sim$4 km,

A gravity wave with a horizontal wavelength of 4 km and a period of 0.5 hour has a phase speed of 2.2 m See^{-1}, Waves generated at the surface with doppler-shifted phase speeds higher than $\sim$2.2 m see^{-1} will be strongly evanescent throughout the troposphere. For example, a wave with a phase speed" of 2.2 m see-l and horizontal wavelength of 4 km has a vertical attenuation scale height at the 10 km level of only 1.6 km, so that the energy of such a wave would be reduced by a factor of 10 for every 2 kilometers of upward propagation, Hence, gravity waves with a horizontal wavelength of 4 km require doppler-shifted phase speeds less than $\sim$2.2 m sec^{-1} to penetrate the troposphere into the stratosphere with significant energy. Waves of the same wavelength with phase speeds below $\sim$2 m see-l make a transition from being evanescent to freely propagating somewhere below the 20 km altitude level; the lower the phase speed, the lower the altitude at which this transition takes place.

Zonal cyclostrophic winds measuring a few meters per second in the troposphere or stratosphere, with vertical shears leading to wind differences of a few meters per second at different altitudes, would have a serious disruptive effect on zonally propagating waves with phase speeds of 2 m see^{-1} or less. Waves propagating in the same direction as the zonal wind would rapidly encounter a critical layer and be absorbed. Waves propagating in the direction opposite to the zonal wind would be rapidly doppler-shifted to frequencies that experience significant vertical attenuation, Hence, unless the zonal wind vertical shear is very weak, the freely propagating waves inferred by HT to exist in the upper troposphere and stratosphere must have been propagating in the meridional plane.

To summarize, the above considerations focus our attention on gravity waves with the following properties, The region of low static stability in the troposphere limits the phase speeds of interest to less than 2 m scc^{-1}. The likely presence of appreciable zonal winds in the troposphere and stratosphere requires that these waves propagated in the meridional direction. HT's results indicated gravity waves at the 44 km level with vertical wavelengths of $\sim$1 km and horizontal wavelengths of $\sim$4 km, implying phase speeds of $\sim$1 m see-l . Because the horizontal wavelength and absolute phase speed of a meridionally and vertically propagating wave packet is nearly conserved in Titan's atmosphere, the horizontal wavelength and phase speed of three waves near the ground should also be 4 km and 1 m see-l .

c. Numerical Model

The equations used to determine the motion of two-dimensional, non-hydrostatic, finite-amplitude gravity waves propagating through a compressible background atmosphere are based on a form of the anelastic equations that ensures that linearized solutions grow with height as $\rho_0^{-1/2}$, where ρ_0 is the basic state density (Bacmeister and Schoeberl 1989). Following Fritts (1978), we express these equations using a streamfunction-vorticity-potential temperature representation, The equations for the wave vorticity and potential temperature are:

$$\frac{\partial \eta'}{\partial t} + \overline{v}\frac{\partial \eta'}{\partial y} + \frac{1}{\rho_0}\frac{\partial \psi'}{\partial y}\frac{\partial \overline{\eta}}{\partial z} + \frac{1}{\rho_0}[J(\psi', \eta') - \overline{J(\psi', \eta')}] + \frac{g}{\theta_0}\frac{\partial \theta'}{\partial y} - \nu\nabla^2\eta' + \beta\eta' = 0 \qquad (1)$$

$$\frac{\partial \theta'}{\partial t} + \overline{v}\frac{\partial \theta'}{\partial y} + \frac{1}{\rho_0}\frac{\partial \psi'}{\partial y}\frac{\partial \overline{\theta}}{\partial z} + \frac{1}{\rho_0}[J(\psi', \theta') - \overline{J(\psi', \theta')}] - \kappa\nabla^2\theta' = 0 \qquad (2)$$

where the Jacobian is defined as

$$J(\phi, \chi) \equiv \frac{\partial \phi}{\partial y}\frac{\partial \chi}{\partial z} - \frac{\partial \phi}{\partial z}\frac{\partial \chi}{\partial y}$$

and where ψ' satisfies

$$\rho_0\eta' = -\nabla^2\psi' + \frac{1}{\rho_0}\frac{d\rho_0}{dz}\frac{\partial \psi'}{\partial z} \qquad (3)$$

Here, y is the coordinate in the meridional direction (positive northward), z is altitude, ρ_0 is the basic state density, $\eta \equiv \frac{\partial v}{\partial z} - \frac{\partial w}{\partial y}$ is the vorticity, θ is the potential temperature, and ψ is the mass strearnfunction, that is

$$\rho_0 v = -\frac{\partial \psi}{\partial z}$$

$$\rho_0 w = \frac{\partial \psi}{\partial y}$$

where v is the northward velocity and w is the vertical velocity. The dynamical variables are divided into a horizontal mean value and a perturbation about this mean,

$$\chi(y,z,t) = \overline{\chi}(z,t) + \chi'(y,z,t)$$

$$\overline{\chi}(z,t) = \frac{1}{L}\int_0^L \chi(y,z,t)dy$$

where L is the fundamental harmonic of the forcing spectrum. ν and κ represent small amounts of momentum and heat diffusivit y, respectively. The term involving β in Eq. (1) is introduced to incorporate a sponge layer at the top of the model to mimic a radiation boundary condition. A term $\eta(\frac{\partial v}{\partial y} + \frac{\partial w}{\partial z})$ has been neglected in Eq. (1). This term is expected to be small whenever the vertical wavelength of the wave is small compared to $4\pi H$, a condition that is well satisfied for the gravit y waves under consideration (Dunkerton and Fritts 1984).

The evolution of the background meridional velocity and potential temperature under the influence of the propagating gravity waves is given by

$$\frac{\partial \overline{v}}{\text{at}} = \overline{?\text{J})\text{q}'} = -\frac{1}{\rho_0}\frac{\partial}{\partial z}\rho_0\overline{w'v'} \qquad (4)$$

$$\frac{\partial \theta}{\partial t} + \frac{1}{\rho_0}\overline{J(\psi',\theta')} - \kappa\nabla^2\overline{\theta} = 0 \qquad (5)$$

For the numerical experiments presented in this study, changes of the background wind and potential temperature were assumed negligible.

Equations (1), (2), and (3) are solved by Fourier expansion in the horizontal and finite differencing in the vertical. The Fourier expansion takes the form

$$\chi'(y,z,t) = \sum_{n=1}^{N}\chi_n(z,t)\text{e}^{inly} + \sum_{n=1}^{N}\chi_{-n}(z,t)\text{e}^{-inly} \qquad (6)$$

where ψ', η', and θ' are to be substituted for χ' and $1 = 2\pi/L$ is the meridional wavenumber of the forced fundamental mode of wavelength L. Substitution of the Fourier expansions into equations (1), (2), and (3) yields the evolution equations for the nth Fourier coefficient:

$$\frac{\partial \eta_n}{\partial t} + \overline{v}\frac{\partial \eta_n}{\partial y} + \frac{1}{\rho_0}\frac{\partial \psi_n}{\partial y}\frac{\partial \overline{\eta}}{\partial z} + \frac{1}{\rho_0}\sum_{\substack{m=-N \\ in-ml<N \\ m\neq 0,n}}^{N} J(\psi_m,\eta_{n-m}) + \frac{g}{\overline{\theta}}\frac{\partial \theta_n}{\partial y} - \nu\nabla^2\eta_n + \beta(z)\eta_n = 0 \qquad (7)$$

$$\frac{\partial \theta_n}{\partial t} + \bar{v}\frac{\partial \theta_n}{\partial y} + \frac{1}{\rho_0}\frac{\partial \psi_n}{\partial y}\frac{\partial \bar{\theta}}{\partial z} + \frac{1}{\rho_0}\sum_{\substack{m=-N \\ in-ml<N \\ m\neq 0,n}}^{N} J(\psi_m, \theta_{n-m}) \quad \kappa\nabla^2\theta_n = 0 \tag{8}$$

$$\rho_0\eta_n = \frac{1}{\rho_0}\frac{d\rho_0}{dz}\frac{\partial \psi_n}{\partial z} - \nabla^2\psi_n \tag{9}$$

The above equations are written in a shorthand form where partial differentiation with respect to y is to be understood as equivalent to multiplication by inl for the nth Fourier coefficient.

Equations (7) and (8) actually comprise $6N$ equations for the time evolution of the Fourier coefficients at each vertical level z. For the calculations described in this paper, N was taken to be 4. Higher values of N were computationally too burdensome. These equations are solved numerically by finite-differencing in the vertical and time. The leapfrog scheme is used to represent all first derivative terms in time and height. The first and second derivatives appearing in Eq. (9) are represented by centered differences, and the resulting linear system is solved by inversion of a tridiagonal matrix, The dissipative terms appearing in Eqs. (7) and (8) are lagged one time step for purposes of computational st ability (Fritts 1978). The model grid extended from Titan's surface to a height of either 154 or 230 km, depending on the requirements of the numerical experiment. Typically, 1600 grid points in the vertical were used, giving Az = 0.15 km or less. The horizontal width of the model domain is given by L, the fundamental harmonic of the forcing at the lower boundary.

Periodic boundary conditions are imposed for the meridional direction, Mechanical forcing of wavelength *L is* established at the lower boundary in the form

$$w'(y, 0, t) = f(t)w_0\sin\left[\frac{2\pi(y - ct)}{L}\right] \tag{10}$$

where c is the meridional phase speed and

$$f(t) = \begin{cases} \frac{t}{t_f} & t < t_f \\ 1 & t \geq t_f \end{cases}$$

is a time ramp function that switches the forcing on slowly to inhibit the introduction of large amplitude transients. t_f is chosen to be 3 wave periods. A "sponge layer" of excess frictional damping is introduced at the uppermost levels of the model to mimic a radiation

boundary condition for the waves (Walterscheid and Schubert 1990). The functional form of the drag coefficient $\beta(z)$ in this layer is taken to be (Klemp and Lilly 1978)

$$\beta(z) = \begin{cases} \frac{0.2}{\Delta t}\sin^2\left(\frac{\pi}{2}\frac{z-z_s}{z_T-z_s}\right) & z \geq z_s \\ 0 & z < z_s \end{cases} \tag{11}$$

with z_s = 97 km and z_T = 154 km or z_s = 165 km and z_T = 230 km.

d. Convective Adjustment

As gravity waves propagate upward through a motionless background atmosphere, conservation of energy requires that their amplitude grow with altitude predominantly as $\rho_0^{\frac{1}{2}}$. A height will eventually be reached where the wave amplitude has grown sufficiently large that the total (wave plus mean) potential temperature gradient becomes negative over some portion of the wave. At this altitude and above, the wave will suffer irreversible convective breakdown. To include this effect in the present model, we make use of a local convective adjustment scheme devised by Dunkerton and Frit ts (1984).

The adjustment procedure works as follows. After each time step of the model, the spectral representations of the variables η' and θ' are Fast Fourier Transformed (FFT) to physical space, forming $2N+1$ equally spaced vertical columns within the fundamental wavelength L. Each column is then inspected for a connectively unstable potential temperature profile. One or several unstable layers may occur within a column. Should they occur, a new equilibrium potential temperature profile $\theta_E(y,z)$ is created from the original profile $\theta_{old}(z)$ by replacing the unstable layers (and a small portion of the adjacent stable layers) with isentropic (that is, constant θ) layers whose upper and lower boundaries are defined by where the isentrope intersects the original profile. The additional requirement to conserve the mass-weighted potential temperature in the column then serves to define a unique equilibrium profile (Dunkerton and Fritts 1984). The vorticity $\eta(y,z)$ is also mixed during the adjustment process; values of η are replaced by their average over each set of vertical grid points affected by the adjustment of θ. The averaging is done in such a way as to conserve the mass-weighted vorticity $\rho_0\eta$ of the unstable layer. Once the convective equilibrium profiles of θ and η are defined, new potential temperature and vorticity profiles are determined for each column by the frictional relaxation formulas

$$\theta_{new} = (\alpha\Delta t)\theta_E + (1 - \alpha\Delta t)\theta_{old} \tag{12a}$$

$$\eta_{new} = (\alpha\Delta t)\eta_E + (1 - \alpha\Delta t)\eta_{old} \tag{12b}$$

Following Dunkerton and Fritts (1984), $\alpha\Delta t$ is chosen to be 0.125. Finally, $\theta_{new}(y,z)$ and $\eta_{new}(y,z)$ are FFTed back to Fourier space in preparation for the next model time step.

3. Results

In this section we present results of numerical calculations for three classes of wave propagation. We first consider a small-amplitude, linear wave packet with sufficiently small phase speed that it suffers no vertical attenuation in the atmosphere. Such a packet is analogous to the freely propagating gravity waves of HT. Second, we investigate propagation of small-amplitude linear gravity waves of somewhat higher phase speed that are evanescent in the lower troposphere. This experiment is intended as a quantitative test of Ross et al.'s hypothesis. We then compute the propagation and evolution of waves that break at some altitude in the model, to determine to what extent wave breaking can provide an explanation for the characteristics of the vertical profile of scintillation index at low altitudes.

a. Small Amplitude, Freely Propagating Wave Packet

If a wave packet is forced at the surface with sufficiently small amplitude, such that its horizontal velocity remains small compared to its doppler-shifted phase speed at all altitudes, then nonlinearity will not play a significant role in its propagation. Also, for sufficiently small-amplitude forcing, the altitude where the wave breaks will lie above the upper boundary of the model, so that the wave will be dissipated in the sponge layer before reaching its breaking level. Hence, for weak forcing, the propagation of a wave packet is well approximated by linear theory. If, in addition, the vertical wavelength of the packet is short compared to the characteristic depth scale over which the background thermal structure changes and its period is short compared to the time scale for changes of the background structure, then WKB theory should provide an accurate approximation of the wave propagation.

In the first numerical experiment, we investigated the propagation of a small amplitude wave packet forced at the surface. The period of the forcing was chosen long enough to ensure that the packet would not be evanescent in the troposphere. A wave of phase speed 1.2 m see^{-1} was forced mechanically at the lower boundary of the model according to Eq. (10), with amplitude w_0 = S.0 cm see--l and horizontal wavelength L = 4 km, The top of the model was placed at 154 km, and the sponge layer extended above 97 km. The grid possessed 1600 equally spaced points in the vertical, and a time step of 25 seconds was employed. Figure 2 shows the development of this wave over four times. The wave propagated upward with a vertical group velocity of approximately 50 cm see–l , and by an elapsed time of *139* h, a steady wave has been established over the entire altitude range. The envelope of the wave train displays the characteristic $\rho_0^{-1/2}$ growth of amplitude with height of a freely propagating packet, modified to a small extent by the altitude variation of the background Brunt frequency, The wave was damped quickly above 97 km by the sponge layer. The vertical flux of northward momentum associated with the developing wave is shown in Figure 3 for the four times depicted in Figure 2. The progression of the wave front with altitude appears clearly in this figure, where unsteady conditions at the leading edge of the wave train lead to a nonvanishing vertical gradient of momentum flux. At low altitudes, where there has been time for steady conditions to be established,

the gradient of the momentum flux with altitude is zero, as expected for a steady, linear, conservative wave. By 139 h, a steady wave solution has been achieved everywhere below the sponge layer, and the momentum flux is seen to be constant with altitude.

In a motionless background atmosphere, and in the absence of appreciable dissipation, the energy density associated with a wave packet satisfies a conservation relation, so that after the wave has become steady, the energy flux of the packet must be constant with altitude. (In an atmosphere with a background wind that varies with altitude, it is wave action flux, rather than the energy flux, that would be constant with height). For a linear wave in a motionless background atmosphere, there is equipartition of kinetic and available potential energy, and the energy density per unit mass can be written $\mathcal{E} = g^2\overline{\rho'^2}/(\rho_0^2 N^2)$, where p' is the perturbation mass density of the wave, The vertical group velocity of the packet is $W_g = lc^2/N$, where c is the meridional phase speed and $1 = 2\pi/L$ the meridional wavenumber. The energy flux in the WKB approximation is then

$$\rho_0 W_g \mathcal{E} = \frac{lc^2}{N}\frac{g^2}{N^2}\frac{\overline{\rho'^2}}{\rho_0} = \text{constant} \qquad (13)$$

It follows from Eq. (13) that for constant wave energy flux $\overline{\rho'^2} \propto p_o N^3$. Since the scintillation index σ^2 is directly proportional to the variance of atmospheric density fluctuations (HT), Eq. (13) also implies $\sigma^2 \propto \rho_0 N^3$. This analytic profile for the scintillation index is shown in Figure 4. Note that σ^2 is approximately constant with altitude below 30 km for this freely propagating wave, in disagreement with the data. Also shown is the synthetic, numerically computed scintillation index profile for the small-amplitude wave displayed in Figure 2, determined by setting $\sigma^2 = C\overline{\rho'^2}$, where p' is the density fluctuation of the wave and C is a constant of proportionality. The amplitude of the wave solution shown in Figure 2 was chosen to give $\rho'/\rho_0 \simeq 7 \times 10^{-4}$ at 44 km, which is in agreement with the result of HT. If a wave of this amplitude was responsible for producing the scintillations observed above 30 km, then the value of C would have to be 5.0×10^{11} cm^6 gin-2 to produce good agreement between the model σ^2 and the data at 44 km, C is a function of geometrical parameters that remained constant during the radio occultation experiment, and is also a weak function of parameters describing the shape of the spatial power spectrum of the irregularities [cf. Eqs. (2) and (3) of HT]. Consequently, C would be approximately constant with altitude if the spatial power spectrum of the density irregularities did not vary strongly with altitude. We have assumed this to be the case for the results that follow. The scintillation index of the analytic solution $\sigma^2 \propto p_o N^3$ is also defined only to within a constant of proportionality; the analytic profile shown in Figure 4 was multiplied by a constant factor to force agreement with the numerical solution at 44 km altitude. The numerical calculation and the analytic solution based on the WKB approximation are found to be in excellent agreement. Also shown in the figure are the scintillation index determined from the radio occultation data by HT and HT's analytic model for freely propagating gravity waves. As noted by HT, the scintillation data falls off with altitude below 30 km much faster than is allowed by the free propagation model. Figure 4 shows

that the the analytic profile derived from Eq. (13) and that of HT can be made to agree well above 70 km and between 30 and 55 km, but in that case the HT profile exhibits larger σ^2 between 55 and 70 km despite the fact that both analytic profiles were derived from energy conservation considerate ions, The discrepancy stems from HT's assumption that the amplitude of vertical displacement for a wave that maintains a constant vertical energy flux grows with height exactly as $\rho_0^{-1/2}$, implying the scintillation index varies $\propto \rho_0 N^4$. Eq. (13) shows, however, that the vertical group velocity varies inversely with N, leading to displacement amplitude growing with height as $p_0^{-1/2} N^{-1/2}$ and σ^2 varying as $p_0 N^3$. This result was also found by Hinson and Magalhaes (1991). Despite this discrepancy between the analytic profiles, their good fit to the data above 65 km reinforces HT's interpretation that freely propagating gravity waves were responsible for the scintillations at high altitudes. It is interesting that the analytic profile of HT appears to provide a better fit to the data between 60 and 70 km (particularly for the higher signal-to-noise X-band data, see Fig. 7 of HT) than does the analytic solution derived here. The reason for this is not clear. HT's profile would be reproduced from Eq. (13) if it were assumed that the group velocity is independent of height, an effect that has been seen in some numerical experiments of the transient development of gravity waves which are allowed to interact with the background flow (Walterscheid and Schubert 1990). In the numerical experiments of this study, the background flow is held fixed. Perhaps the gravity waves on Titan modified the mean meridional flow in such a way that the vertical group velocity was maintained constant with height, Future numerical experiments which incorporate acceleration of the background flow by the waves may be able to test this conjecture.

b. Evanescence in the Troposphere

The dispersion relation for gravity waves of doppler-shifted angular frequency ν, horizontal wavenumber 1 and vertical wavenumbcr m is given by

$$m^2(z) + \frac{1}{4H^2} = l^2\left(\frac{N(z)^2}{\nu^2} - 1\right) \tag{14}$$

The equation has been written in a form that emphasizes the low pass filter characteristic of the lower troposphere of Titan, where N is small. Where ν exceeds the local value of N, the wave is evanescent, and its energy density varies with height like $\exp(z/H - 2|m|z)$. It was suggested by Ross et al. (1989) that a frequency or spectral range may exist where $|m|$ has the correct value to reproduce the vertical profile of σ^2 in the lower troposphere. Waves in this spectral range would be partially attenuated in the troposphere but would reach the upper troposphere where they become vertically propagating traveling waves with sufficient amplitude to account for the scintillation data at high altitudes.

Closer examination of this hypothesis reveals that it is untenable. The scintillations measured by the radio occultation experiment owe their existence to rapid variations in the refractive index over scales of a few hundred meters to a few kilometers. Evanescent waves, on the other hand, vary smoothly with height. Hence the vertical component of

motion of the radio ray path through an" evanescent wave could not have produced the rapid intensity scintillations seen in the troposphere. However, the possibility that the scintillations were produced by the horizontal motion of the ray path through such a wave, which varies sinusoidally in the horizontal, must also be considered, The horizontal velocity of the ray through the atmosphere during the occultation was $v_y \simeq$ 0,1 km see–l, and the experiment was sensitive to signal variations with frequencies lying in the spectral range ω =1-10 Hz, This implies that the horizontal wavelength L of any evanescent wave causing signal variations in the correct frequency range must satisfy $L < v_y/\omega_{min}$ = 100 meters.

For gravity waves with horizontal wavelengths less than 100 m propagating through a motionless atmosphere, the explanation of the low altitude scintillation profile in terms of vertical attenuation is undone by the vertical variation of N with altitude. To fit the average trend of the scintillation data below 30 km requires a nearly uniform value of $*3 \times 10^{-7}\ cm^{-1}$ for the decay constant $|m|$, corresponding to a decay scale length $|m|^{-1}$ of about 1.5 pressure scale heights. Inspection of Eq. (14) reveals that this value of $|m|$ will occur only in the extremely narrow region where $N(z)$ differs from ν by no more than about one part in 10^7 For example, for *L = 100 m,* the same wave frequency required to match $|m| = 3 \times 10^{-7}\ cm^{-1}$ at 20 km, where N = $3{,}7 \times 10^{-3}$ see-l, yields $|m| \simeq 3.2 \times 10^{-4}\ cm^{-1}$, or a decay scale of only $\sim 10^{-3}$ scale height, at the 10 km level where N = 3.2×10^{-3} s e e^{-1}. For waves with wavelength shorter than 100 m, the attenuation is even more severe. Consequently, it is impossible to fit the average trend of the scintillation data with vertically attenuated waves with horizontal wavelengths less than 100 m. If the tropospheric scintillations are to be accounted for by gravity waves, a mechanism other than evanescence must be found to slow the growth of their amplitude with height.

c. Breaking Waves

The amplitude of a steady linear wave grows with altitude approximately exponentially as $\rho_0^{-1/2}$ in order to maintain a constant energy flux. This growth with altitude can not continue indefinitely, however. At some altitude, the perturbation potential temperature of the wave will have become so large that the total (wave plus mean) potential temperature profile will be unstable to convection over some horizontal portion of the wave. Previous work has shown that the effect of convective breakdown of the wave is to strongly limit or entirely stop further growth of amplitude with height (Lindzen 1981; Walterscheid and Schubert 1990). Walterscheid and Schubert have shown that convective breakdown can even affect the amplitude growth with height of a transient, developing wave at altitudes far below the breaking level. Since the vertical profile of scintillations below ~30 km is consistent with waves which maintain an approximately constant amplitude as they travel upward, 'it is natural to investigate the effects of wave breaking on the scintillation profile.

In the following numerical runs, the amplitude of forcing at the lower boundary was chosen large enough to ensure that the wave would break somewhere below the sponge layer of the model. The altitude at which breaking first occurs, z_b, can be estimated from the formula (Andrews et al. 1987)

$$z_b \sim 2H \ln \frac{c}{v_0} \qquad (15)$$

where V. is the amplitude of the horizontal velocity forced at the surface, As a consequence of continuity, $lv_0 \sim$ *n-tw,, so* that Eq. (15) can also be regarded as a relationship between z_b and W.. Unfortunately, it was generally not possible to follow the evolution of the breaking wave system for arbit rarily long integration times, Breaking has the propensit y to introduce successively smaller vertical scales into the atmospheric structure as time evolves, and eventually these scales decreased below the vertical resolution of the model, leading to numerical instability, Consequently, the numerical results for breaking waves are presented only for times where it was clear that the fine structure of the system was adequately resolved by the model grid.

It will be instructive to first present the results for the case where wave breaking occurs at high altitude. The temporal behavior illustrated by this case is common to all the calculations where breaking occurred. Figure 5 shows the vertical profile of σ^2 for four times during the development of a wave for which W.= 6 cm see^{-1} . The phase speed of the forced wave was taken to be 3 m see-l and the horizontal wavelength was taken to be 20 km. The phase speed of 3 m See-l was chosen to reduce the computational burden in this calculation, which otherwise would be quite demanding (note that the vertical group velocity is proportional to the square of the phase speed), and the wavelength of 20 km was chosen to ensure that t hc wave would not be evanescent. For W. = 6 cm sec $^{-1}$, Eq. (15) implies that the breaking level ought to be located roughly near the 130 km level. Actually, breaking occurred near 150 km. After an elapsed time of 144 hours (panel a), the scintillation index has essentially the vertical profile of a freely propagating wave packet (cf. Fig. 2). At 192 hours, the profile begins to show signs that the wave has broken at high altitude, As discussed below, the high wavenumber structure in the profile is duc to interference between the incident wave and downward propagating harmonics of the incident wave generated in the breaking region by the convective adjustment process. After 217 hours, the model profile begins to exhibit relatively high values of σ^2 at low altitudes while closely following the free propagation profile at high altitudes. However, the decrease of the average value of σ^2 with altitude is slower than that of the data, and the calculated values of σ^2 between 30 and 60 km are somewhat too high. By an elapsed time of 240 hours, the shape of the model σ^2 profile is quite different from that of the data below 60 km, The solution for 240 hours does not represent a steady state solution, and indeed no steady solutions were found for numerical runs in which wave breaking played a role,

The scintillation profiles for all times shown in Figure 5 were scaled by a constant factor to force agreement between the model and data at 44 km. This was necessary because the fractional density variation ρ'/ρ_0 engendered by the wave forced with an amplitude of w_0 = 6 cm see-l was $\sim 3 \times 10^{-3}$ at 44 km, about a factor of 3 larger than the value derived by HT, producing values of σ^2 about a factor of 9 larger than the data. Assuming equipartition of kinetic and available potential energy in the wave, it can be shown that

the fractional density scales as $(1+\frac{m^2}{l^2})^{1/2} w_0$. This, together with Eq. (15), implies that a wave with $L = 20$ km which breaks near 150 km and produces a fractional density variation at 44 km of 10^{-3} should have an amplitude $w_0 \simeq 0.7$ cm See–l and a phase speed of 1 m sec^{-1}. Because the vertical group velocity of the 1 m see-l wave is only of the order of 5 cm sec^{-1}, a relatively large amount of time would be required for the wave packet to reach 150 km, break, and continue evolving, and hence a long model integration time would have been necessary. Such a long integration time was too computationally burdensome to be undertaken at this time. As a consequence, in this and the following numerical experiment, we have focused on the shape of the model scintillation profile, implicitly assuming that this shape depends primarily on the altitude level of breaking and only weakly on the choice of phase speed and amplitude of the wave. This expectation is verified below for the numerical experiment in which wave breaking occurs near 15 km.

The temporal evolution of the propagating, breaking wave whose scintillation index is shown in Figure 5 is best followed by examining the altitude profile of the wave vertical momentum flux $\rho_0 v' w'$ as a function of time. The background dissipation in this numerical experiment was negligible, so the momentum flux of a steady, linear, conservative wave should be independent of height. Figure 6 shows the evolution of the vertical momentum flux profile for several times during the wave propagation. At a time of 72,2 hours, the leading edge of a wave train is apparent in the vertical momentum flux at the 100 km level. Behind the leading edge of the wave train, at lower altitudes, the wave has had time to become approximately steady, as reflected by the nearly constant vertical momentum flux. By 95.8 hours, however, breaking of the wave is apparent in the destruction of the leading edge at 150 km and above. The wave amplitude above the breaking level is limited by convective instability, which is here treated through local convective adjustment of the wave plus mean flow field. The wave vertical momentum flux decreases approximately $\propto \rho_0$ above the breaking level,

The local, convective adjustment in the breaking region introduces harmonics of the forced primary wave, since in the unstable phase of the wave (which comprises only a section of the total wavelength of the wave) the potential temperature and vorticity are reset to adiabatic and well-mixed values, respectively, while in the stable portion of the wave they are left unchanged. The harmonics are free to propagate both upward and downward from the breaking region. Those propagating downward carry a downward momentum flux which partially cancels the upward momentum flux of the primary wave. This behavior is very similar to that found in a study of gravity wave breaking conducted by Bacmeister and Schoeberl (1989). These authors found that wave breaking caused a large reduction of the vertical momentum flux of the flow not only at the breaking level, but also at lower altitudes, and they attributed over half of the reduction in momentum flux to downward propagating waves which were generated in the breaking region, Essentially the same behavior is exhibited in Figure 6 after t = 95.8 hours. The "destruction" of the primary wave momentum flux can be traced as it travels downward with a speed of $\sim$0.5 m see^{-1} between t = 95,8 hours and t = 239.7 hours. This speed is approximately the group velocity of a wave with the same frequency of the primary wave but with half the horizontal and vertical wavelengths. Superposition of the downward propagating harmonics with

the primary wave leads to a complicated interference pattern which shows up as small scale oscillatory structure in the scintillation and momentum flux vertical profiles. The appearance of large σ^2 at low altitudes after t = 217 hours coincides with the arrival and reflection of the downward propagating waves at the surface. The effect of breaking has trapped some portion of the incident wave energy below the breaking level, leading to enhanced values of scintillation index at low altitude.

While wave breaking at high altitude offers a mechanism for creating relatively large scintillation index at low altitudes, it is clear that the solution shown in Figure 5 does not provide a good fit to the data at altitudes below 60 km. The average gradient with altitude of the calculated σ^2 tends to follow that of the free propagation curve, that is, σ^2 approximately constant with altitude. This indicates that wave amplitudes at low altitudes in this run were not independent of altitude, but instead increased with height approximately as $\bar{\rho}_0^{-1/2}$. Walterscheid and Schubert (1990) demonstrated that wave breaking and transience can combine to severely limit wave amplitude growth at altitudes well below the level of breaking, but that effect has not come into play here. The effect depends on inhibition of the buildup of wave kinetic energy by nonlinear processes; however, nonlinearity has played only a weak role at low altitudes in the present calculation because wave perturbation velocities at low altitudes are small compared to the wave phase speed.

Wave amplitudes at low altitudes on Titan might have remained nearly constant with height due to breaking at low altitude. As indicated by Eq. (15), this requires a larger ratio of wave perturbation velocity to phase speed near the surface than that of the previous experiment. Figure 7 shows the results of a simulation for a wave with L = 4 km, c = 1.5 m see-l and w_0 = 75 cm see–l . Breaking occurred at an altitude of $\sim$15 km. The fit to the low altitude σ^2 data is fairly good, in particular the general gradient of σ^2 with height is reproduced, but above 30 km the model completely fails to capture the free propagation regime. This failure stems from the fact that the wave field is saturated (constant amplitude with height) above the breaking region. In addition, the model scintillation index shown in Figure 7 was scaled to force agreement with the data at 5 km, The actual value of the scintillation index computed was a factor $\sim$245 too large at 5 km, implying an overestimate of the fractional density variation by a factor of about 15.

The scintillation data at 5 km require $\rho'/\rho_0 \simeq 2 \times 10^{-4}$. In order for a L = 4 km wave to reproduce this fractional density fluctuation at 5 km and break at or below 15 km, it must have a phase speed of c $\simeq$ 20 cm see-l and amplitude $w_0 \simeq 1.4$ cm sec^{-1} . Figure 8 shows the scintillation index profile computed using these parameters. The integration was carried out on a grid with 3200 grid points extending between the surface and 68 km, with the sponge layer lying above an altitude of 51 km. Since the computational burden of this numerical experiment was relatively high, the wave evolution could be followed only for a short time, and the wave front had travelled no higher than the 30 km level by the end of the calculation. This explains the sharp drop in the model σ^2 occurring just above 30 km in the figure, The wave was found to first break close to the 15 km level. As for the case shown in Figure 4, the model scintillation index was calculated using the formula $\sigma^2 = C\overline{\rho'^2}$, where C = 5.0 x 10^{11} cm^6 gm^{-2}, The large-scale variation of the data

with altitude below 25 km is approximately recovered by the model, although the altitude where the scintillation index peaks is placed slightly too high, and the model scintillation index is a factor of ~1.5 too low below 15 km, As with the case shown in Figure 7, the small scale structure in the data below 25 km is not reproduced, and the high altitude scintillation data can not be simulated by the breaking wave.

d. Combination of Freely Propagating and Breaking Waves

The results presented above demonstrate that the high altitude scintillation index can be simulated by a freely propagating wave with a horizontal wavelength of 4 km and phase speed of 1.2 m sec^{-1}, while the low altitude scintillation index can be simulated by a breaking wave with a horizontal wavelength of 4 km and phase speed of 20 cm see-l . However, neither wave by itself can simulate the scintillation index over the entire altitude range of the observations. It is therefore desirable to determine whether a better solution can be obtained with a slightly more complex model in which both waves are forced at the lower boundary simultaneously. One would expect the freely propagating wave, with its much larger vertical group velocity, to race ahead of the slower breaking wave, establishing the high-altitude scintillation index profile before the slower component has had a chance to break at low altitude. Since the breaking component would be saturated above its breaking level, it would not contribute significantly to the scintillations at high altitudes, Similarly, the freely propagating wave would make only a minor contribution at low altitudes. To test this conjecture, a calculation was performed in which both waves were forced simultaneously at the lower boundary. The amplitude of the freely propagating wave was set at w_0^f = 8.0 cm see–l and the amplitude of the breaking wave was set at w_0^b = *1.4* cm see^{-1}. The phase speed of the breaking component was taken to be 18 cm see^{-1}. The result for the simulated scintillation index is shown in Figure 9. The model fit to the large-scale structure of the data is now quite good over the entire altitude range between 5 and 85 km, although the model produced too small an index near 70 km. This failure to accurately reproduce the correct ratio between the scintillation indices at ~40 and 70 km was encountered previously in the calculation involving only the freely propagating wave, and the origin of this discrepancy is unknown, Again, the model dots not reproduce the large "spikes" seen in the scintillation index at low altitudes. These spikes may originate from rapid density variations occurring on small scales that are not resolved by the model. Such variations may arise as the result of the superposition of waves having slightly different vertical wavelengths. Alternatively, they may be associated with the relatively large density changes that accompany strong overturning in a breaking wave (cf. Walterscheid and Schubert 1990).

4. Discussion

The calculations described in the previous section represent an effort to ascertain whether surface-generated gravity waves could have been responsible for creating the observed scintillations over the entire range of altitude from the surface to the 90 km level. The behavior of the scintillation data with altitude is different below and above the ~25

km level. Below, the data imply that the amplitude of gravity waves that might be responsible for the scintillations must remain approximately constant with altitude, Above, their amplitude must increase with altitude predominantly as $\rho_0(z)^{-1/2}$. Numerical calculation of the propagation of a small-amplitude wave packet that does not suffer wave breaking or vertical attenuation in the model domain produced a scintillation index profile that was generally in good agreement with the data between 30 and 85 km except in a layer between 65 and 75 km, confirming HT's analytic model for freely propagating gravity waves for this altitude range. The discrepancy between the present model calculation and the data between 65 and 75 km may be attributable to neglect in the model of the acceleration imparted to the background meridional wind by the passing waves, although this is uncertain. The discrepancy between the model calculation and HT's analytic model stems from their neglect of the dependence of the wave vertical group velocity on the background buoyancy frequency. The small-amplitude wave packet calculation and HT's analytic model both fail to reproduce the general trend of scintillation index at low altitudes, underestimating the magnitude of the scintillations by nearly an order of magnitude.

Evanescent waves, driven above the cutoff frequency of the lower troposphere, also can not account for the observed scintillation profile, Since these waves vary smoothly with height, any scintilla ions they might have caused would have to have been created by the horizontal component of motion of the radio ray path through the atmosphere. This fact restricts the horizontal spatial scales of the density irregularities to which the scintillation experiment was sensitive to less than approximately 100 meters. Waves with horizontal wavelengths this short decay much too quickly with altitude in the troposphere to match the data.

Attempts to model the low-altitude profile in terms of breaking gravity waves were more successful. Waves which break at an alt itude near 15 km produce a profile in good agreement with the data below 30 km, but fail to reproduce the high-altitude scintillation profile, largely because the calculated wave amplitudes remain saturated (that is, constant with height) above the breaking level, A model in which both a freeI y propagating component and a breaking component are forced at the surface generally produces a good fit to the large-scale structure of the data in the entire altitude range between 5 and 90 km, although some nagging discrepancies remain. It is almost certain that this model oversimplifies the actual nature of the gravity wave event that produced the observed scintillations on Titan, For example, the actual wave train may have included a full spectrum of phase speeds lying below about 1.5 m see–l . Nevertheless, the overall success of the simulation is a strong argument that gravity waves were responsible for the scintillations in both the troposphere and stratosphere, with the properties of the waves given approximately by the parameters derived here.

To fit the observed fractional density fluctuation of $\rho'/\rho_0 \sim 10^{-3}$ at the 44 km level, a freely propagating packet must be forced at the surface with an amplitude of $w_0 \sim 8.0$ cm see–l , A wave which produces the correct magnitude for the low altitude scintillations breaks at 15 km and has a phase speed of $\sim$20 cm see-l and amplitude $w_0 \sim 1.4$ cm see–l , assuming its horizontal wavelength is about 4 km. The question naturally arises as to how

waves of the amplitudes cited above might be forced at the surface of Titan. Two possible mechanisms for exciting the waves at the surface are convective forcing and flow of the atmosphere over topography, Consider convective forcing first, In the lowest few kilometers of Titan's atmosphere, the solar and thermal infrared heat which reaches the surface must be carried upward by convection. This upward energy flux has been estimated to be on the order of 1 W m^{-2} (Hunten et al. 1984), The vertical energy flux associated with the freely propagating waves with amplitude $w_0 \sim 8$ cm see-l and phase speed ~ 1 m sec^{-1} is about 7×10^{-3} W m^{-2}, or roughly 0.7% of the convective energy flux that is available for generation of the gravity waves. This efficiency is comparable in magnitude to estimates for the efficiency with which equatorially trapped waves are excited by convective processes on Earth (Andrews et al, 1987), but the significance of this comparison is devalued by the fact that the equatorially trapped waves are of much greater spatial scale than the gravity waves being modeled here, and so may have a markedly different efficiency for excitation. An additional argument can be made in support of generation of the freely propagating waves by convective heating near the surface. The vertical temperature profile determined by the RSS radio occultation experiment (Lindal et al. 1983) displays a nearly adiabatic lapse rate up to an altitude of 3-4 km and quickly becomes subadiabatic above. As Hunten et al. (1984) point out, the nearly adiabatic lapse rate marks a region of buoyancy-driven turbulence forced by heating at the surface. Numerical calculations of the generation of gravity waves on Earth by a mixed convective boundary layer (Kuo and Sun 1976) indicate that the largest amplitude waves have horizontal and vertical wavelengths approximately equal to the depth of the layer. Hence we would expect the mixed layer of depth ~ 4 km on Titan to generate gravity waves with horizontal and vertical wavelengths of ~ 4 km. This horizontal wavelength is in agreement with the analysis of HT. A wave with vertical wavelength of 4 km in the statically stable atmosphere just overlying the mixed layer, at an altitude of 4 km where $N \sim 2.4 \times 10^{-3}$ See-l, has a phase speed given by Eq. (14) of 1.1 m see-l , in good agreement with the phase speed of the gravity waves modeled by HT. Given the present uncertainties in the model and in our general understanding of convective generation of gravity waves, it is not yet possible to determine unambiguously whether the freely propagating gravity waves modeled here and by HT originated from convective forcing.

The vertical energy flux associated with the breaking wave component is approximately 1.5×10^{-3} W m^{-2}, so again the convective heat flux appears to be adequate for convect ive generation of this component. However, there is no immediate physical argument that can be offered to explain the phase speed and wavelengths of the breaking wave. More information concerning the properties of the strong scintillations at low altitudes, particularly their dominant vertical and horizontal spatial scales, would undoubtedly be helpful in resolving this problem. This information will become available in the future when strong scat tering theory is applied to the Voyager 1 RSS scintillation data set (HT).

Alternatively, the gravity waves might have originated from topographic forcing at Titan's surface. The efficacy of this type of forcing is more difficult to evaluate within the context of the present model, since the assumption has been made that the background meridional wind is negligible and that the waves have nonzero phase speed with respect

to the ground. Topographically forced plane waves, on the other hand, must have zero phase speed with respect to the ground, the nonzero doppler-shifted phase speed of the disturbance arising entirely from the motion of the background atmosphere, To be consistent with the observations, stationary plane waves would have to propagate through a background meridional wind of ~ 1 m see–l . Such a large mean meridional wind is not expected on theoretical grounds, and in any event, it would be expected to have a strong disruptive effect on the wave propagation if it possessed a modest amount of vertical shear (see Sect ion 2). Therefore, it seems unlikely that stationary gravity waves with doppler-shifted phase speeds of 1 m See-l were forced by flow of the meridional wind over topography. However, meridionally traveling waves could have been produced by flow of the *zonal* wind over an isolated obstacle of finite meridional extent. In this more realistic, three-dimensional case, wave modes with nonzero cross-stream (i.e., meridional) wavenumbers would carry energy horizontally north and south away from the obstacle, An estimate can be made of the topographic relief required to force waves with the energy fluxes given above. The answer will be uncertain, however, as it depends on the static stability of the mixed layer in the lowest ~ 4 km of the atmosphere, which is poorly known, and on the degree to which the forced wave is reflected at the discontinuity in static stability occurring near the 4 km level. A rough estimate for the static stability of the mixed layer can be obtained using the occultation data of Linda] et al, (1983), and we find $N \simeq 6 \times 10^{-4}$ See–l. This value is probably uncertain by a factor of about 5. Because N is small in the mixed layer, waves with horizontal wavelength of 4 km or less and phase speeds greater than 40 cm see–l are vertically trapped. Hence, the freely propagating waves with $c \simeq 1$ m sec $^{-1}$ would be evanescent in the mixed layer, but the breaking component, with $c \simeq 20$ cm sec^{-1} , would not be. The net wave energy flux that ultimately escapes the mixed layer depends on the degree of reflection occurring at the discontinuity in static stability at the 4 km level, which in turn depends on the number of quarter wavelengths occurring between the ground and the discontinuity (see Gill, 1982). This number is not known. However, a range of values for the topographic relief can be given for the extreme cases of strong and weak reflection. To produce a wave energy flux of 1.5×10^{-3} W m^{-2} for the breaking component, topographic relief of about 60 m is required if there is onl y weak reflection and about 300 m is required if there is strong reflection. These numbers are based on the formula

$$h_0^2 = \frac{2\mathcal{F}}{\rho_0} \times \begin{cases} \frac{1}{kc^3 m_2} & \text{weak reflection} \\ \frac{1}{kc^3 \frac{m_2^2}{m_1}} & \text{strong reflection} \end{cases} \qquad (16)$$

where *ho* is the height of an obstacle forcing the wave, $\mathcal{F}$ is the wave energy flux, *p.* = 5.6×10^{-3} gm cm^{-3} is the density at the surface, $k = 1.57 \times 10^{-5}$ cm–l and $c = 20$ cm see^{-1} are the horizontal wavenumber and phase speed of the wave, and $m_1 = 2.6 \times 10^{-5}$ cm^{-1} and $m_2 = 1.3 \times 10^{-4} \mathrm{cm}^{-1}$ are the vertical wavenumbers in the mixed layer and the adjacent overlying atmosphere, respectively. The Brunt frequency was taken to be 6×10^{-4} see-l in the mixed layer and 2.4×10^{-3} sec. $^{-1}$ above. Therefore, to the extent

that this model for the" stratification is accurate, it seems that modest topographic relief lying between about 60 and 300 meters would have been sufficient to force the breaking wave component, but the freely propagating component would have been vertically trapped in the mixed layer.

Absorption of the vertical flux of northward momentum carried upward by the gravity waves might conceivably make an important contribution at high altitudes to the balance of forces acting in the meridional direction. In the absence of stresses exerted by waves, the north-south gradient of geopotential is expected to be balanced primarily by the centrifugal force acting on the zonal wind u (Hunten et al. 1984). The meridional balance of forces can be written as

$$\frac{tan\Lambda}{R_T}u^2 = -\frac{1}{R_T}\frac{\partial\Phi}{\partial\Lambda} + f_\Lambda \qquad (17)$$

Here, A is the latitude, R_T is the radius of Titan, Φ is the geopotential, and f_Λ represents forces in the meridional direction exerted by friction or by eddies. When f_Λ is ignored, Eq. (17) is reduced to expressing cyclostrophic balance between the zonal wind and the geopotential gradient. The freely propagating wave packet that best fits the scintillation data at altitudes above 30 km carries upward a vertical flux of northward momentum $\tau \simeq 0.02$ g cm-l sec^{-1}. This wave will break near the 150 km level, where the pressure is ~ 3 mbar. In the upper stratosphere, u has been estimated to be on the order of ~ 75 m sec^{-1} (Hunten et al, 1984), and the latitude of the radio occultation ingress was A = 6.2" N, giving a centrifugal acceleration of 0.02 cm sec^{-2}. If it is assumed that the momentum of the vertically propagating wave is absorbed by breaking over a depth of roughly a scale height, as suggested by the results shown in Figure 6, then the wave forcing exerted in the meridional direction can be estimated using the formula $f_\Lambda \sim \tau/(\rho_0 H)$. Since $\rho_0 \simeq 6 \times 10^{-6}$ gm cm^{-3} near 150 km, $f_\Lambda \simeq 1.0 \times 10^{-3}$ cm see^{-2}, or only 5% of the centrifugal acceleration. Hence, the waves causing the high altitude scintillations would not have made a significant contribution to the meridional momentum budget, except possibly within $\sim 1°$ of latitude of the equator.

Acknowledgements

This work was performed by the Jet Propulsion Laboratory, California Institute of Technology, under contract with the National Aeronautics and Space Administration. It was supported by a grant from the NASA Planetary Atmospheres Program.

References

Andrews, D. G., J, R. Holton and C. B. Leovy 1987. *Middle Atmosphere Dynamics.* Academic Press, Orlando.

Bacmeister, J. T. and M, R. Schoeberl 1989. Breakdown of vertically propagating two-dimensional gravity waves forced by orography. *J. Atmos. Sci. 46, 2109.*

Dunkerton, T. J. and D, C. Fritts 1984. Transient gravity wave-critical layer interaction. Part I: Convective adjustment and the mean zonal acceleration. *J. Atmos. Sci. 41,992.*

Flasar, F. M., R. E. Samuelson, and B. J. Conrath 1981, Titan's atmosphere: Temperature and dynamics. *Nature 292, 693.*

Fritts, D. C. 1978. The nonlinear gravity wave-critical level interaction. *J. Atmos. Sci. 35, 397.*

Gill, A. E. 1982. *Atmosphere- Ocean Dynamics.* Academic Press, San Diego.

Hinson, D. and G. L. Tyler 1983. Internal gravity waves in Titan's atmosphere observed by Voyager radio occultation, *Icarus 54, 337.*

Hinson, D.H and J. A. Magalhaes 1991. Equatorial waves in the stratosphere of Uranus. *Icarus 94, 64.*

Hubbard, W. B., B. Sicardy, R. Miles, A. J. Hollis, R. W. Forrest, I. K. M. Nicolson, G. Appleby, W. Beisker, C. Bittner, H.-J. Bode, *et al.*. The occultation of 28 Sgr by Titan. *Astronomy and Astrophysics,* in press.

Hunten, D. M., M. G. Tomasko, F. M. Flasar, R, E, Samuelson, D. F. Strobe], and D. J. Stevenson 1984. Titan. In *Saturn,* T. Gehrels and M. S. Matthews, Eds., (Univ. of Arizona Press, Tucson, 1984), p. 671.

Klemp, J. B. and D. K. Lilly 1978. Numerical simulation of hydrostatic mountain waves. *J. Atmos. Sci. 35, 78.*

Kuo, H. L. and W. Y. Sun 1976. Convection in the lower atmosphere and its effects. *J. Atmos. Sci. 33,* 21.

Lighthill, J. 1978. *Waves in Fluids,* (Cambridge Univ. Press, Cambridge, 1978).

Lindal, G. F., G. E. Wood, H. B, Hotz, D. N. Sweetnam, V. R. Eshleman, and G. L. Tyler 1983. The atmosphere of Titan: An analysis of the Voyager 1 radio occultation measurements. *Icarus* 53, 348.

Lindzen, R. S. 1981. "Turbulence and stress due to gravity wave and tidal breakdown. *J. Geophys. Res. 86,* 9707.

Ross, M. N., G. Schubert, and R, L. Walterscheid 1989. Gravity wave propagation in Titan's atmosphere, *Bull. Am. Astron. Sot. 21, 960.*

Toon, O. B., C. P. McKay, R. Courtin, and T. P. Ackerman 1988. Methane rain on Titan. *Icarus 75, 255,*

Tyler, G. L., V. R, Eshleman, J. D. Anderson, G, S. Levy, G. F. Lindal, G. E. Wood, and

T. A. Croft 1981. Radio science investigations of the Saturn system with Voyager 1: Preliminary results. **Science 212,201,**

Walterscheid, R, L. and G. Schubert 1990. Nonlinear evolution ofan upward propagating gravity wave: overturning, convection, transience, and turbulence. *J. Atmos. Sci.* 47, 101,

Figure Captions

Figure 1. Background atmospheric thermal structure of Titan used in the calculations. (a) Temperature, (b) Brunt frequency.

Figure 2. Development of small-amplitude wave packet over time. The perturbation vertical velocity is plotted as a function of altitude for four times. A steady wave solution was established by 139 h. The grid resolution was 0.096 km for this numerical run, The sponge layer extended above 97 km,

Figure 3. The vertical flux of northward momentum $\rho_0 v'w'$ vs. altitude corresponding to the wave shown in Figure 2. The momentum flux is constant with height at those altitudes below the wavefront where steady conditions have been established.

Figure 4. There are four profiles of scintillation index (σ^2) vs. altitude in this plot. Thin solid line – 13 cm-entry scintillation data produced by Hinson and Tyler (1983), The data above 85 km is dominated by noise. The curve was produced by hand through digitization of their Figure 7. Heavy solid line – numerical solution corresponding to wave shown in Figure 2 at 139 h. Long-dashed line - analytic solution derived from Eq, (13), $\sigma^2 \propto \rho_0 N^3$. Short dashed line - analytic gravity wave model of Hinson and Tyler $(\sigma^2 \propto \rho_0 N^4)$. The error bar represents Hinson and Tyler's estimate of the error in their determination of the scintillation index near 60 km,

Figure 5. Scintillation index profiles for a wave that breaks at 148 km, at elapsed times of (a) 144 h, (b) 192 h, (c) 216 h, and (d) 240 h. Although the solution is not steady, the general trend of the model scintillation profile at low altitude tends to be constant with altitude, in disagreement with the data.

Figure 6. The vertical flux of northward momentum for a wave that breaks at 148 km. The corresponding scintillation profiles for this wave are shown in Figure 5. The grid resolution for this run was 0.4 km. Note the downward propagating destruction of the primary wave, See text for details.

Figure 7. Scintillation index vertical profile for a wave that breaks at an altitude of 15 km. The model scintillation profile. was shifted downward to force agreement between model and data at 5 km,

Figure 8. Scintillation index for a wave with c = 20 cm see-l , L = 4 km, and w_0 = 1.4 cm see-l . The model profile is shown for an elapsed time of 444 h. Unlike the case for Figure 7, no shifting of the model profile was done to force agreement with the data.

Figure 9. Scintillation index for the case where both a breaking wave and freely propagating wave were forced at the lower boundary, Agreement between the model (thick line) and the large-scale structure of the data (thin line) is generally good, except near the 70 km altitude level. The unrealistically small stint illation indices calculated for altitudes above

90 km are the result of the presence of a sponge layer beginning at 90 km which rapidly damped the wave solution above that altitude,

Figure 1 Friedson (199

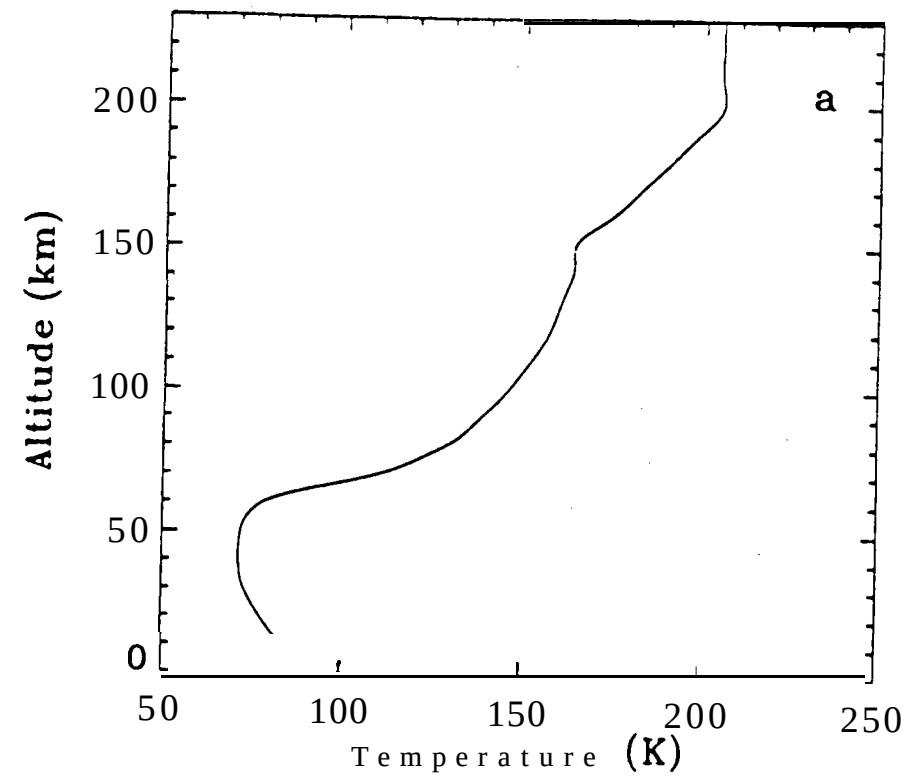

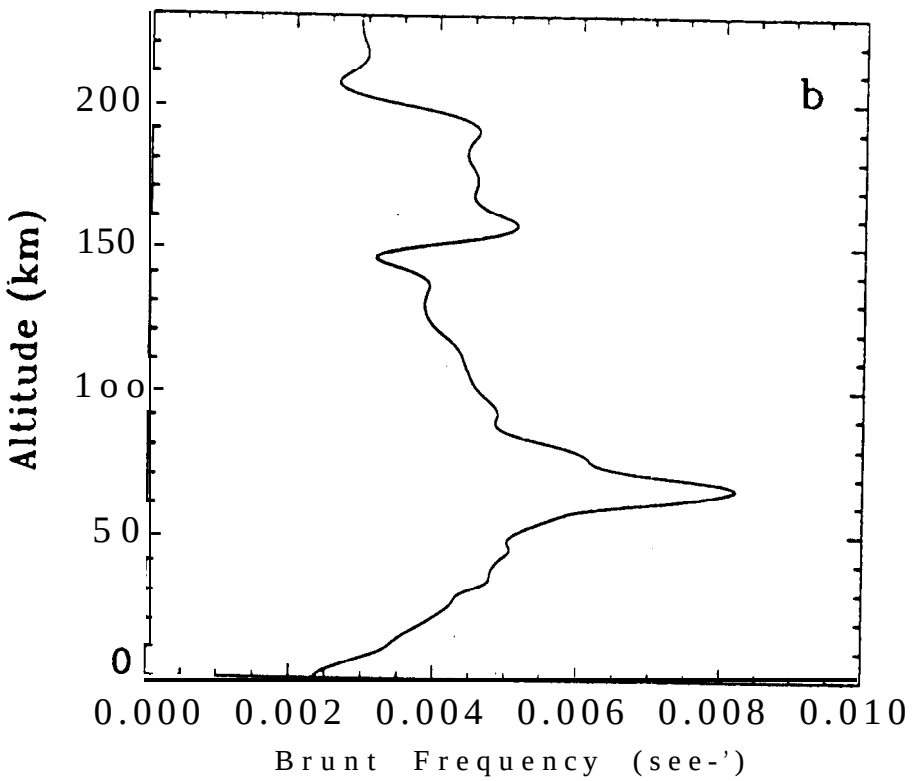

Friedson - Figure 2

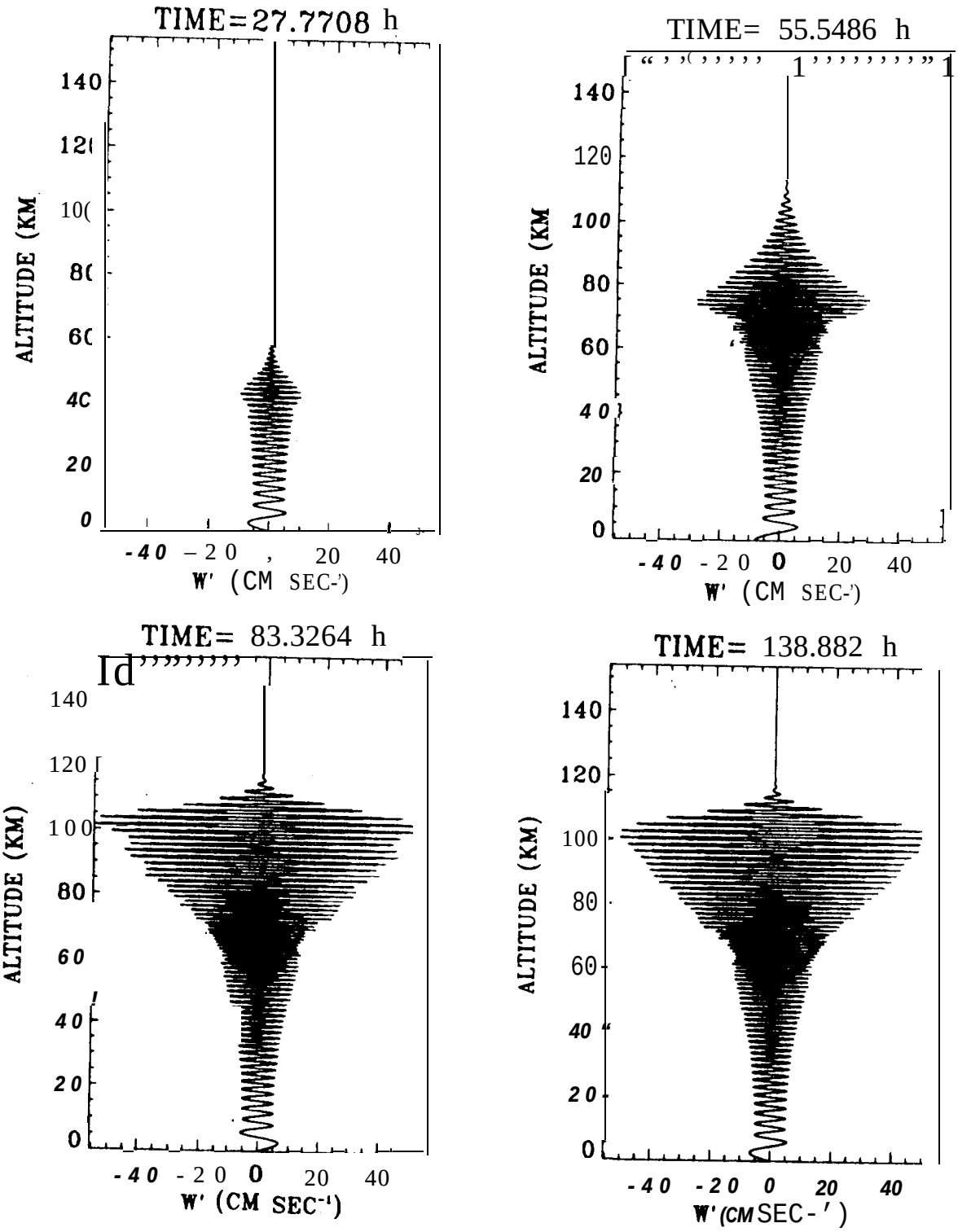

Friedson - Figure 3

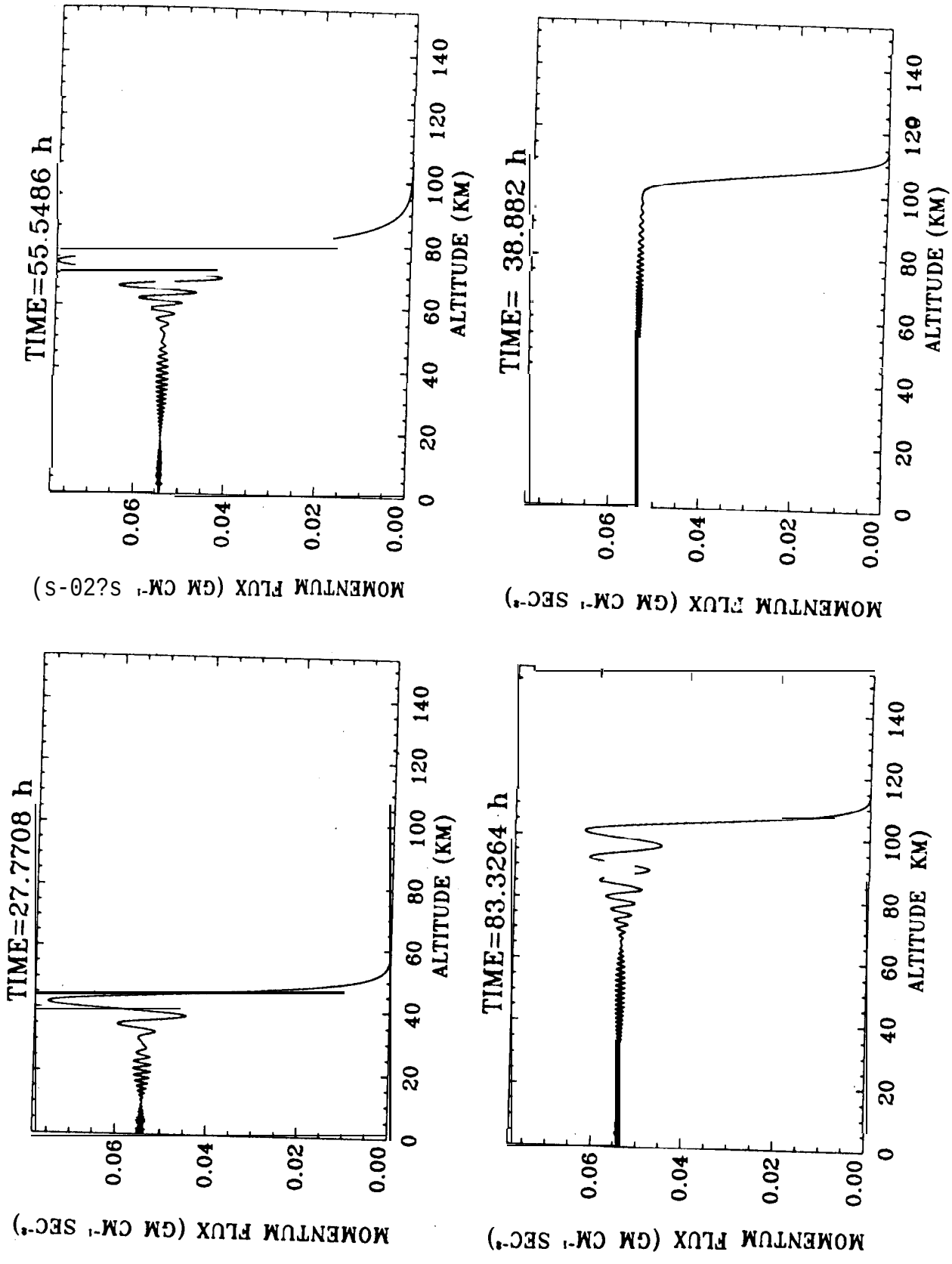

Friedson - Figure 4

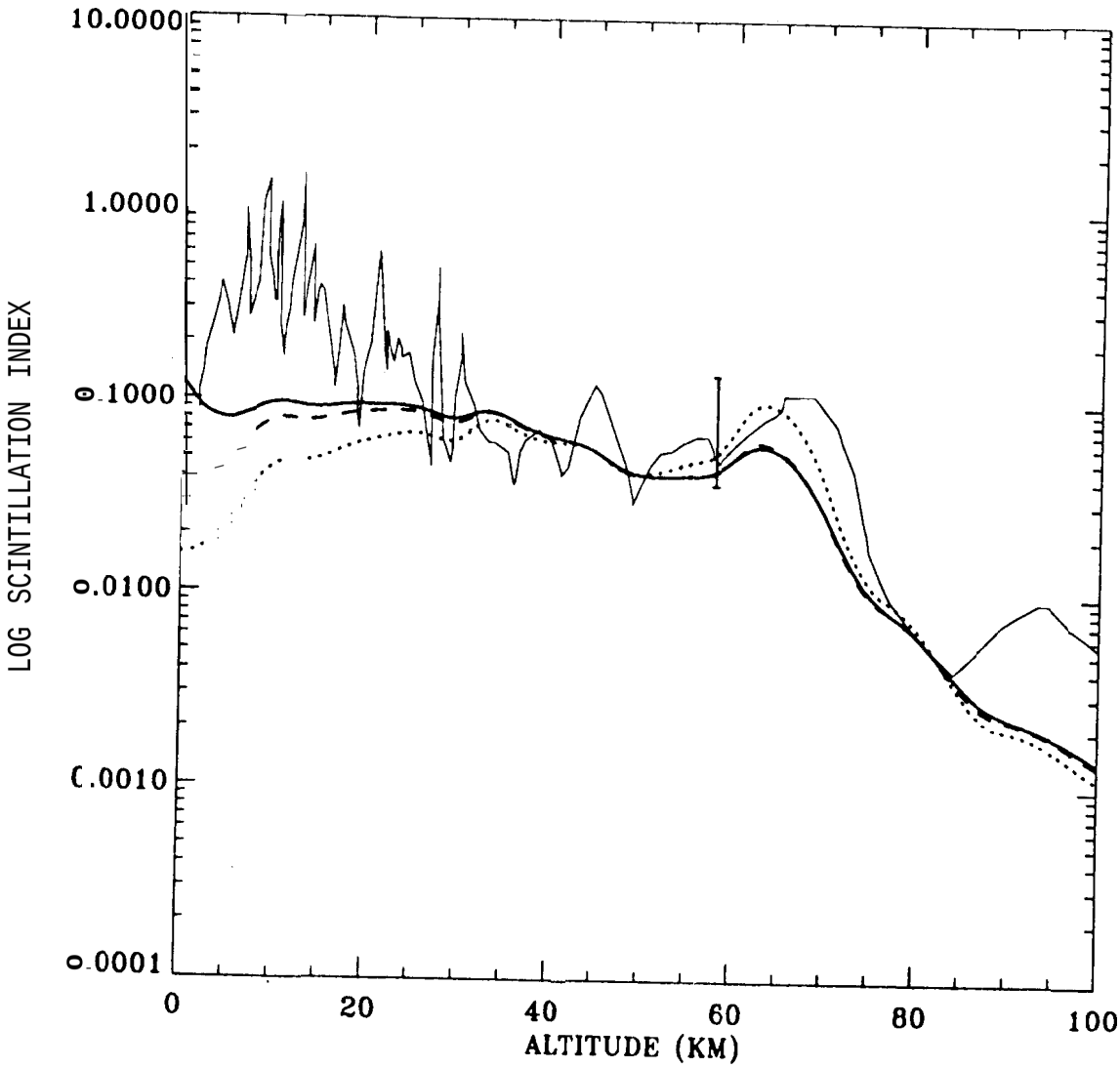

Friedson – Figure 5a

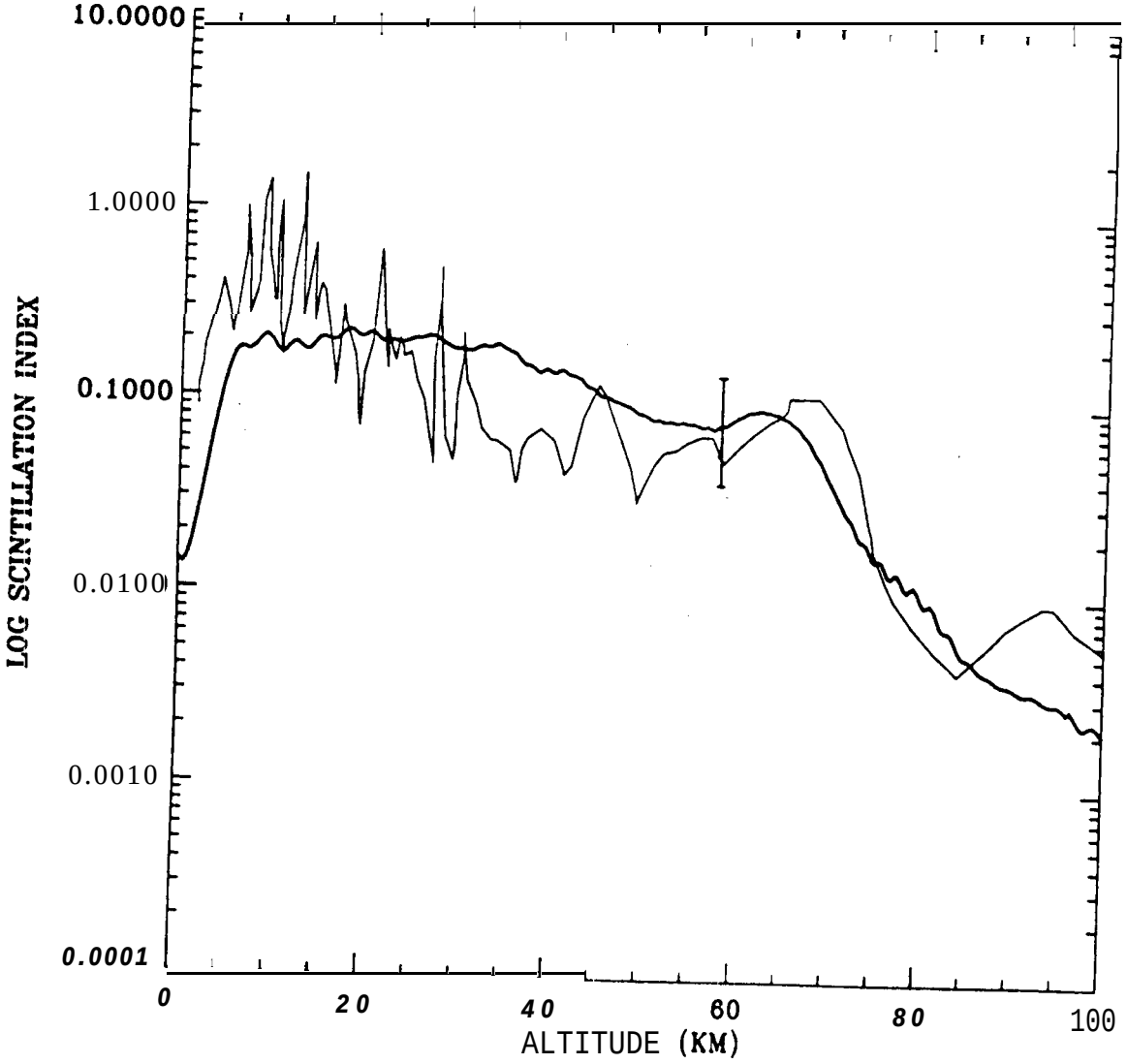

Friedson - Figure 5b

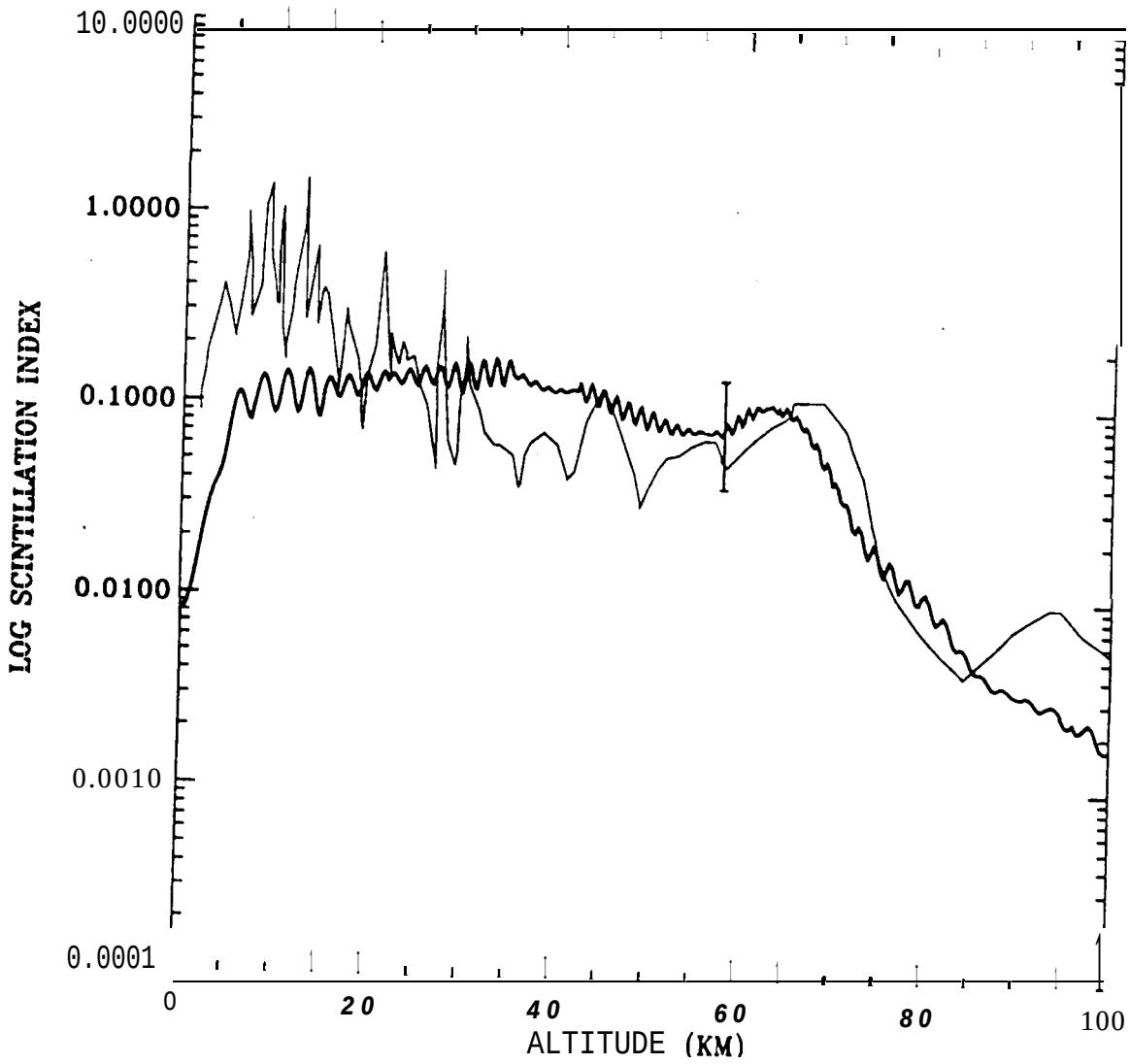

Friedson – Figure 5c

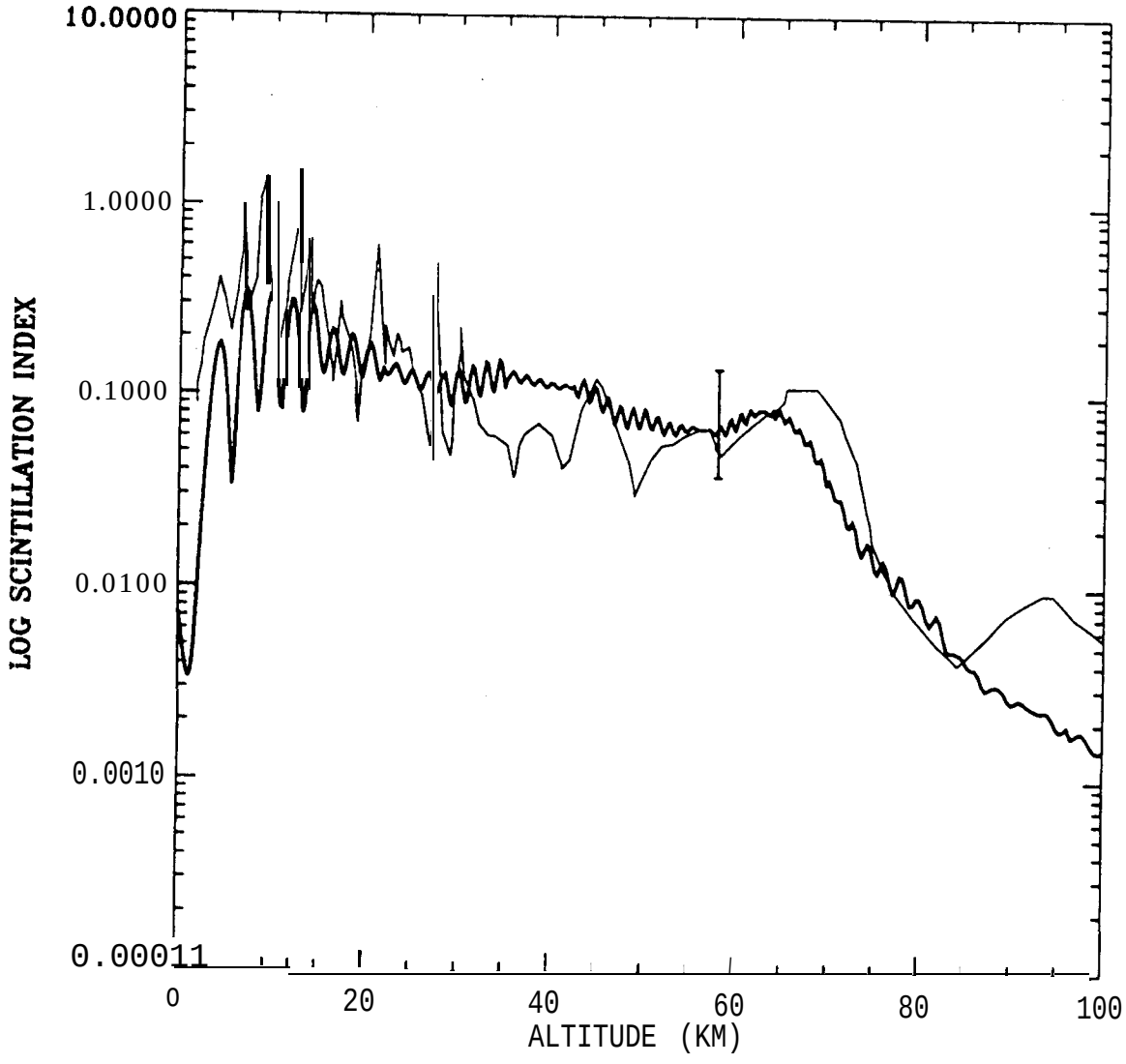

Friedson – Figure 5d

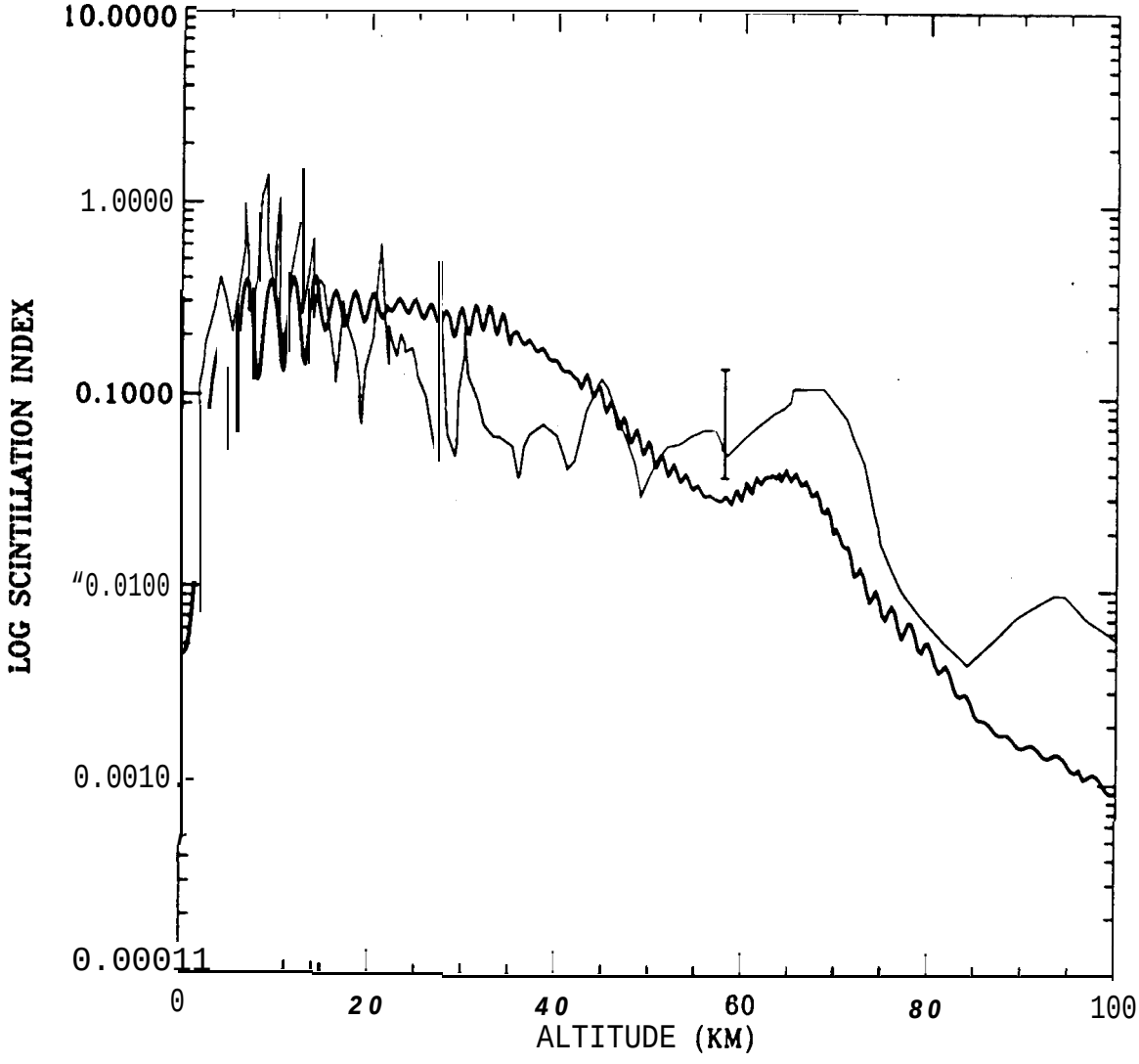

Figure 6

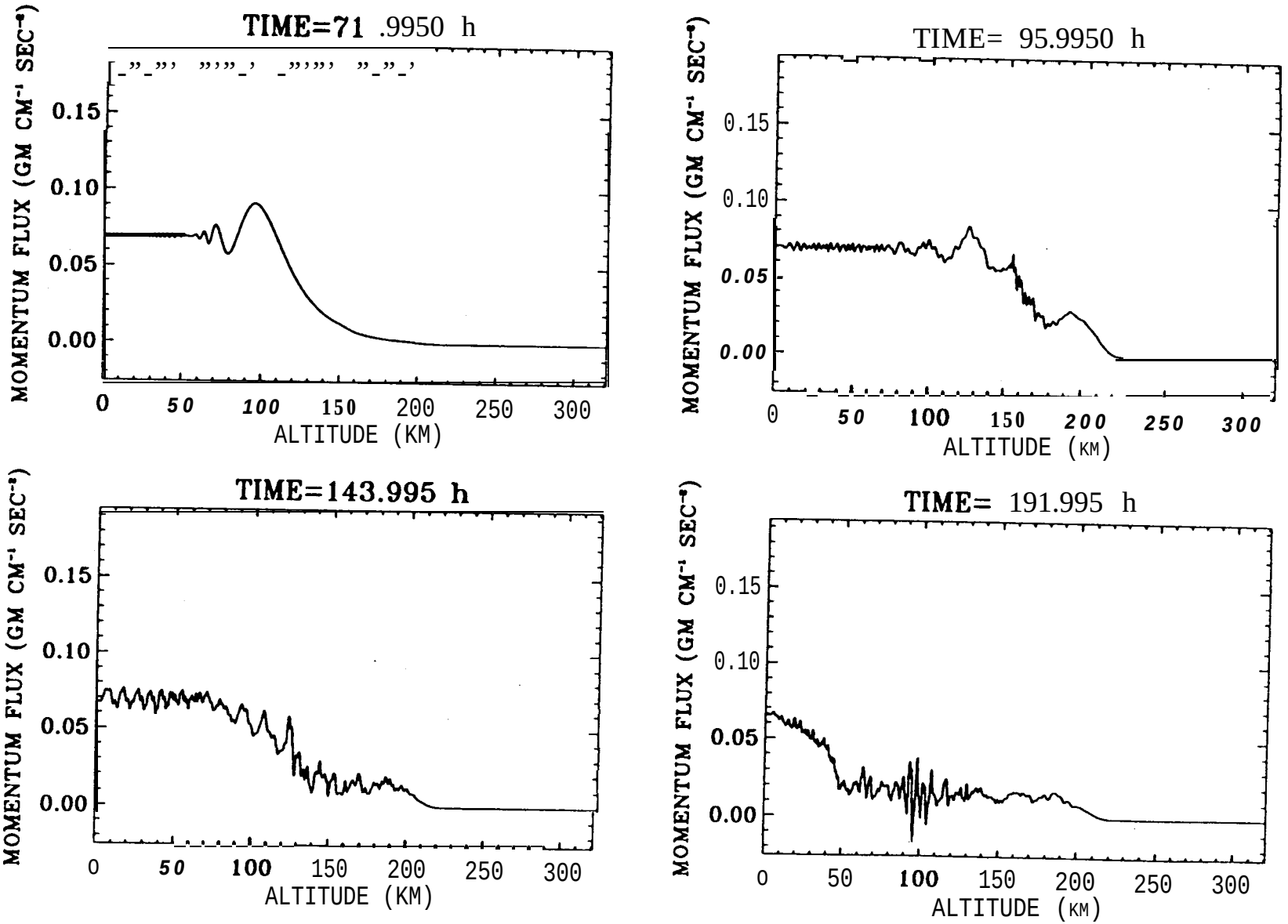

Fritts/Isler - Figure 6

Friedson – Figure 7

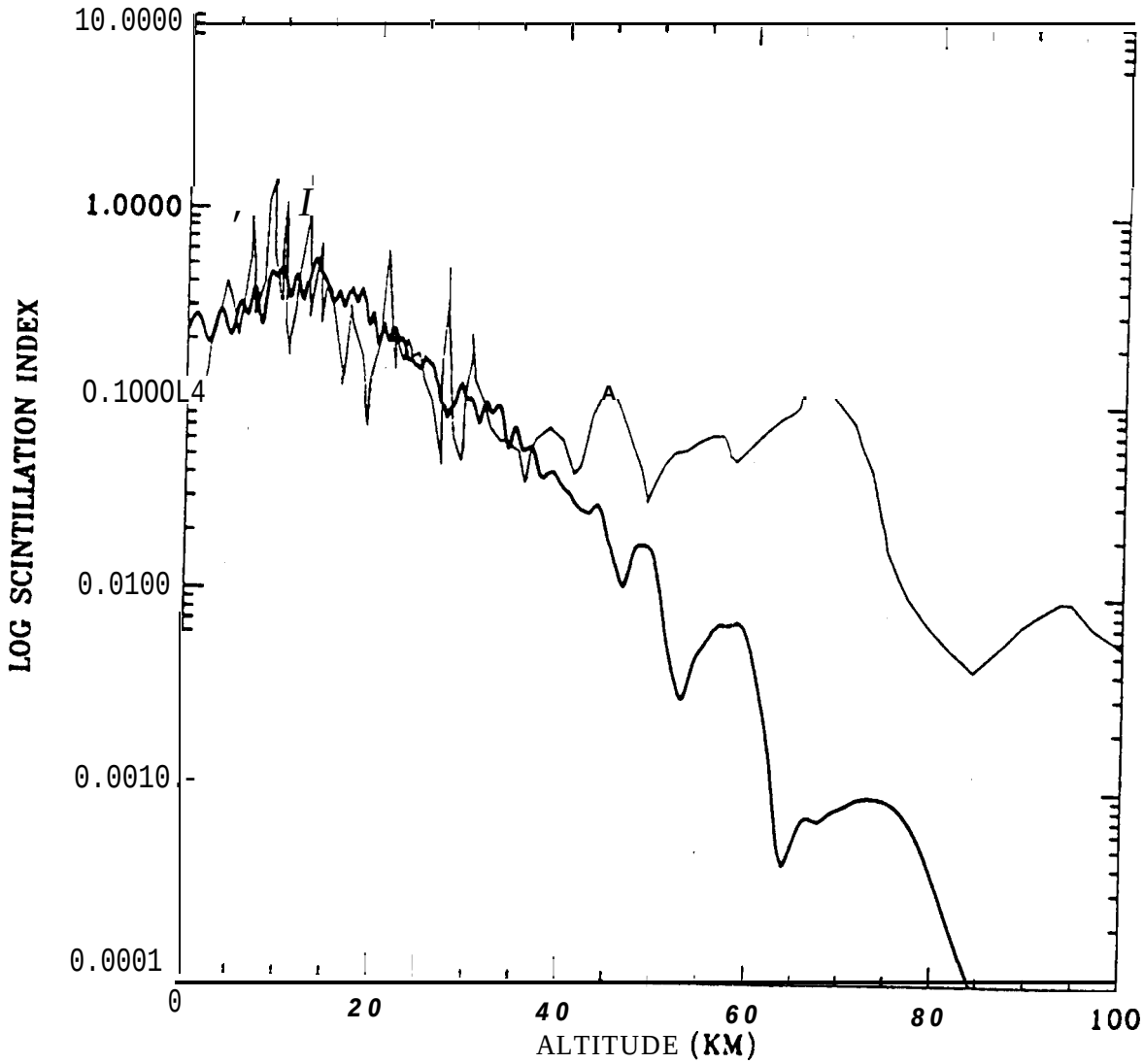

Friedson - Figure 8

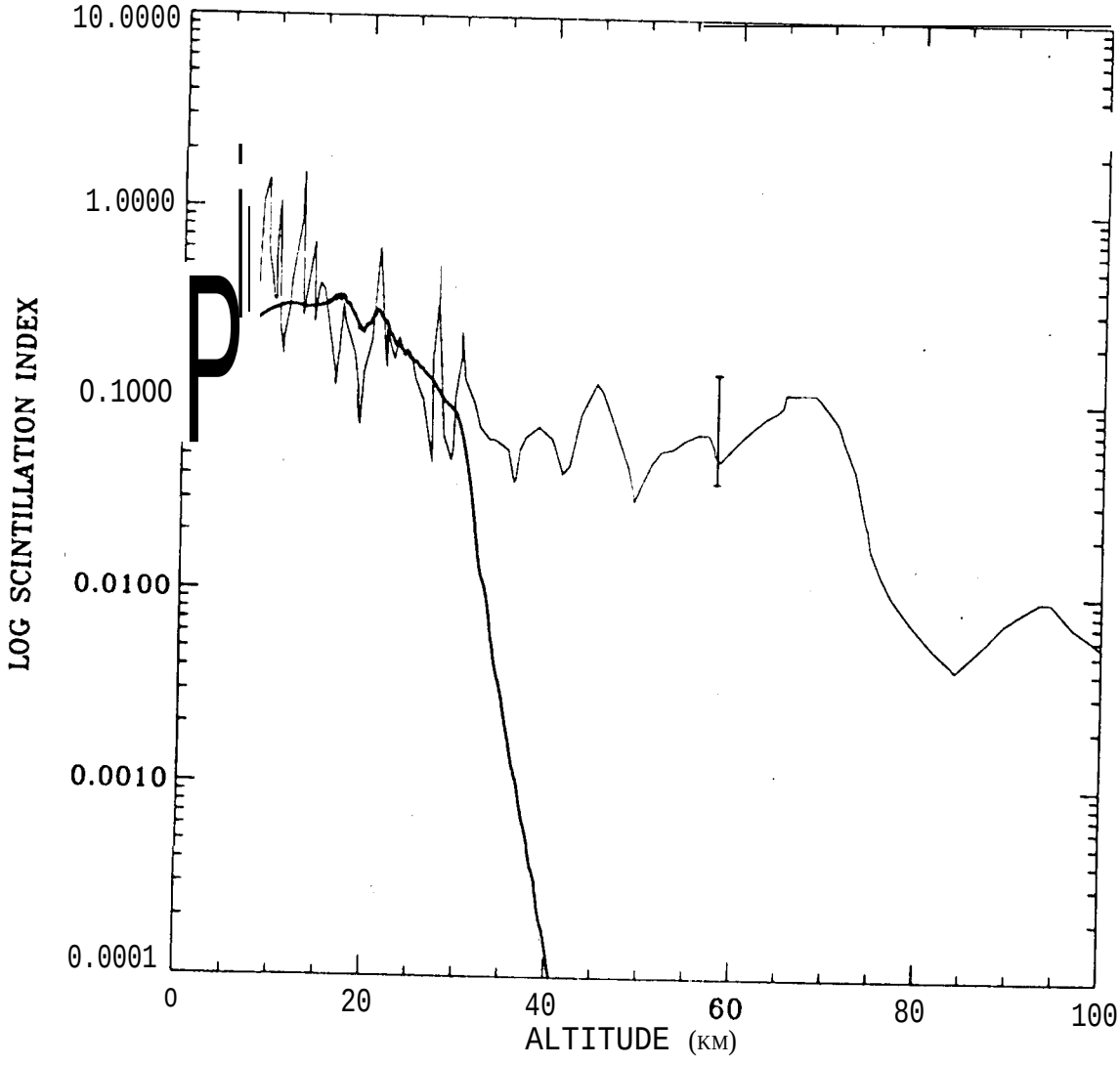

Friedson - Figure